



# Kilometer-scale climate models: Prospects and challenges

Christoph Schär\*

*Atmospheric and Climate Science, ETH Zürich, Switzerland*

Oliver Fuhrer

*Federal Office of Meteorology and Climatology MeteoSwiss, Zürich, Switzerland*

Andrea Arteaga

*Federal Office of Meteorology and Climatology MeteoSwiss, Zürich, Switzerland*

Nikolina Ban

*Atmospheric and Climate Science, ETH Zürich, Switzerland*

Christophe Charpilloz

*Atmospheric and Climate Science, ETH Zürich, Switzerland,  
and MeteoSwiss, Zürich, Switzerland*

Salvatore Di Girolamo

*Computer Science, ETH Zürich, Switzerland*

Laureline Hentgen

*Atmospheric and Climate Science, ETH Zürich, Switzerland*

Torsten Hoefler

**Early Online Release:** This preliminary version has been accepted for publication in *Bulletin of the American Meteorological Society*, may be fully cited, and has been assigned DOI 10.1175/BAMS-D-18-0167.1. The final typeset copyedited article will replace the EOR at the above DOI when it is published.

18  
19  
20  
21  
22  
23  
24  
25  
26  
27  
28  
29  
30  
31  
32  
33  
34  
35  
36

*Computer Science, ETH Zürich, Switzerland*

Xavier Lapillonne

*Federal Office of Meteorology and Climatology MeteoSwiss, Zürich, Switzerland*

David Leutwyler

*Atmospheric and Climate Science, ETH Zürich, Switzerland,  
and Max Planck Institute for Meteorology, Hamburg, Germany*

Katherine Osterried

*Center for Climate Systems Modeling (C2SM), ETH Zürich, Switzerland*

Davide Panosetti

*Atmospheric and Climate Science, ETH Zürich, Switzerland*

Stefan Rüdüsühli

*Atmospheric and Climate Science, ETH Zürich, Switzerland*

Linda Schlemmer

*Atmospheric and Climate Science, ETH Zürich, Switzerland*

Thomas Schulthess

*Swiss National Supercomputing Center (CSCS), Lugano, Switzerland*

Michael Sprenger

*Atmospheric and Climate Science, ETH Zürich, Switzerland*

Stefano Ubbiali

37

*Swiss National Supercomputing Center (CSCS), Lugano, Switzerland*

38

Heini Wernli

39

*Atmospheric and Climate Science, ETH Zürich, Switzerland*

<sup>40</sup> \*Corresponding author address: Atmospheric and Climate Science, ETH Zürich, Switzerland

<sup>41</sup> E-mail: [schaer@env.ethz.ch](mailto:schaer@env.ethz.ch)

## ABSTRACT

42 Currently major efforts are underway towards refining the horizontal reso-  
43 lution (or grid spacing) of climate models to about 1 km, using both global  
44 and regional climate models (GCMs and RCMs). Several groups have suc-  
45 ceeded in conducting km-scale multi-week GCM simulations, and decade-  
46 long continental-scale RCM simulations. There is the well-founded hope that  
47 this increase in resolution represents a quantum jump in climate modeling, as  
48 it enables replacing the parameterization of moist convection by an explicit  
49 treatment. It is expected that this will improve the simulation of the water  
50 cycle and extreme events, and reduce uncertainties in climate-change projec-  
51 tions. While km-scale resolution is commonly employed in limited-area nu-  
52 merical weather prediction, enabling it on global scales for extended climate  
53 simulations requires a concerted effort. In this paper, we exploit an RCM that  
54 runs entirely on graphics processing units (GPUs) and show examples that  
55 highlight the prospects of this approach. A particular challenge addressed in  
56 this paper relates to the growth in output volumes. It is argued that the data  
57 avalanche of high-resolution simulations will make it impractical or impossi-  
58 ble to store the data. Rather, repeating the simulation and conducting online  
59 analysis will become more efficient. A prototype of this methodology is pre-  
60 sented. It makes use of a bit-reproducible model version that ensures repro-  
61 ducible simulations across hardware architectures, in conjunction with a data  
62 virtualization layer as a common interface for output analyses. An assessment  
63 of the potential of these novel approaches will be provided.

## 64 **Capsule summary**

65 Kilometer-resolution climate models provide exciting prospects, as they will explicitly represent  
66 convective clouds. We explore this approach using a limited-area atmospheric model and discuss  
67 prospects, challenges and potential solutions.

## 68 **1. Introduction**

69 While the basic scientific concepts of anthropogenic climate change are now well established,  
70 uncertainties in climate projections have remained staggeringly large. For instance, current esti-  
71 mates of the equilibrium climate sensitivity (ECS) – the equilibrium global surface warming in  
72 response to a doubling of atmospheric CO<sub>2</sub> concentration – are between 1.5 and 4.5 °C. Over the  
73 last 40 years, this uncertainty range, covering a probability of 66%, has not narrowed (Charney  
74 et al. 1979), and according to the most recent IPCC assessment report, even extreme values of  
75 the ECS (below 1 °C and above 6 °C) cannot be excluded (IPCC 2013). This evident uncertainty  
76 makes it difficult to plan for adequate response strategies essential to mitigate the anticipated  
77 warming. Reducing this uncertainty is also of paramount importance in order to provide more re-  
78 liable projections of sea-level rise, regional climate change and extreme events, which are essential  
79 to climate change adaptation.

80 The key reason behind the slow progress in reducing the uncertainties of climate projections is  
81 likely the lack of adequate computational resolution, together with the importance of small-scale  
82 processes in the climate system. In particular, there is evidence that the response of tropical and  
83 subtropical clouds may significantly amplify or reduce global warming, depending upon changes  
84 in cloud reflectivity with global warming (Bony and Dufresne 2005; Sherwood et al. 2014; Schnei-  
85 der et al. 2017, 2019). Likewise, eddy-resolving ocean models are expected to contribute towards  
86 reducing uncertainties in ECS by better representing ocean heat uptake (e.g. Gregory et al. 2002;

87 Ringler et al. 2013; Hewitt et al. 2017), but in the current article we will focus on atmospheric  
88 models.

89 With the advent of emerging supercomputing platforms, and with the progress in high-resolution  
90 climate modeling, there are now promising prospects to refine the horizontal resolution<sup>1</sup> of global  
91 climate models from today's 50-100 km to 1-2 km, thereby explicitly resolving some of the small-  
92 scale convective cloud processes (e.g. thunderstorms and rain showers). There is the well-founded  
93 hope that this increase in resolution might lead to a quantum jump in climate modeling, as it  
94 enables replacing the parameterizations of moist convection and gravity-wave drag by explicit  
95 treatments (Palmer 2014). It is also hoped that this will improve the simulation of the water cycle  
96 and of extreme events, and reduce uncertainties in ECS. However, what resolution will actually  
97 be needed for the later purpose is not yet fully understood. On the one hand, convective cloud  
98 processes (dynamics, turbulence and microphysics) occur on scales that are not fully resolved at  
99 km-resolution (Skamarock 2004; Neumann et al. 2019; Panosetti et al. 2019). On the other hand,  
100 studies have indicated that there is some bulk convergence at grid resolutions around 2 km, i.e. the  
101 feedbacks between convective clouds and the larger-scale flow are partly captured at resolutions  
102 at which the structural details of the cloud field are not yet fully resolved (Langhans et al. 2012;  
103 Harvey et al. 2017; Ito et al. 2017; Panosetti et al. 2018, 2019). Following Schulthess et al. (2018)  
104 and Neumann et al. (2019) we thus assume that a global resolution of 1 km is a suitable near-term  
105 target. Thus further improvements in the parameterizations of the turbulence and microphysical  
106 processes appear essential, as these processes will remain poorly resolved.

107 The development and testing of climate models with horizontal resolutions of around 1 km is  
108 already well underway. Both global and regional models have contributed to this development,  
109 with the former refining the horizontal resolution on a global domain, and the latter expanding

---

<sup>1</sup>In this paper we are using the terms "resolution" and "grid spacing" synonymously.

110 the computational domains of high-resolution limited-area models (Fig. 1). The target (1 km on a  
111 global domain) can be approached both ways. The figure also shows an estimate of the relative  
112 computational costs (green lines), assuming that the vertical resolution is kept constant, where-  
113 upon the number of operations scales with  $N_z A \Delta x^{-3}$ , with  $A$  denoting the horizontal area of the  
114 domain,  $N_z$  the number of vertical levels, and  $\Delta x$  the horizontal grid spacing. This scaling assumes  
115 perfect computational scalability and that the time step is refined together with the horizontal reso-  
116 lution, consistent with maintaining a constant Courant number, a measure for how far information  
117 propagates per timestep relative to the gridspace.

118 Some prototype simulations (e.g. Miyamoto et al. 2013; Fuhrer et al. 2018) are already close  
119 to the target (Fig. 1, right-hand panel), but these models have not yet been run over climate time  
120 periods, but merely over days to seasons. There are also major initiatives on the further devel-  
121 opment of these approaches, such as the Energy Exascale Earth System Model (E3SM)<sup>2</sup> of the  
122 US Department of Energy, or the high-resolution modeling activities at many weather and climate  
123 centers culminating in simulations of 9 atmosphere-only codes at kilometer-scale resolution for a  
124 40-day-long common simulation period (Sato et al. 2019, DYAMOND<sup>3</sup>).

125 In any case, realizing the potential of global convection-resolving climate simulations requires  
126 enormous efforts and innovative solutions at the interface of computer and climate sciences. Some  
127 of these aspects will be addressed in this paper: How can we efficiently leverage the next genera-  
128 tions of supercomputers? What programming languages should we use to make our climate codes  
129 future-proof? How can we overcome the data avalanche generated by high-resolution models?  
130 How can we trade storing the model output with re-computation of model simulations?

---

<sup>2</sup><https://e3sm.org/>

<sup>3</sup><https://www.esiwace.eu/services-1/diamond-initiative>

131 We will discuss these aspects by exploiting a version of the COSMO limited-area model that has  
132 extensively been used at km-resolution in the last decade, and that can be run entirely on modern  
133 supercomputers at unprecedented speed. While this framework is still far away from the global-  
134 domain km-scale target, the main challenges are exposed and potential solutions can be assessed.  
135 Sections 2 and 3 of the paper outlines the main challenges and potential strategies, and Section 4  
136 presents some specific applications and results. The study is concluded in Section 5.

## 137 **2. Challenges of km-scale resolution**

### 138 *a. Exploiting next generation hardware architectures*

139 While high-performance computing (HPC) system performance has continued to increase year  
140 after year<sup>4</sup>, a series of fundamental technology transitions had profound impacts on programming  
141 models and simulation software. After decades of scaling transistor power efficiency, the energy  
142 required to move data has become the dominant performance constraint (e.g., Kestor et al. 2013).  
143 Figure 2 presents the energy consumption for elementary store and compute operations. It illus-  
144 trates the fact that for common operations (reading two double precision floating point numbers  
145 from system memory, performing an addition, and storing the result back into system memory)  
146 the energy required for the data transfers is approximately 100 times larger than that required to  
147 execute the actual arithmetic operation. Finally, energy constraints for large HPC systems have led  
148 to heterogeneous node designs with accelerators such as graphics processing units (GPUs). With  
149 the end of exponential scaling of transistor size towards the end of this decade (often referred to as  
150 Moore's law), disruptive architectural changes and architectural diversity and complexity are ex-  
151 pected to continue to increase. In order to take advantage of the computational power of the largest  
152 HPC systems, climate models have to be able to run on these emerging hardware architectures.

---

<sup>4</sup><https://top500.org>



153 Lacking proper programming abstractions, details of these novel hardware architectures are ex-  
154 posed to the application developer via software libraries (e.g., MPI to handle data movement be-  
155 tween remote memories), extensions to programming languages (e.g., OpenACC compiler direc-  
156 tives for GPU programming) or entirely new programming languages (e.g., CUDA, a language for  
157 GPU programming). The climate modeling community has begun to realize the enormity of the  
158 challenge facing them. A climate model typically has on the order of one million lines of source  
159 code, rendering the traditional programming paradigms and development process unsustainable.  
160 As a consequence, global fully-coupled climate models are not capable of efficiently leveraging  
161 current leadership class HPC systems. The effort required for the maintenance, validation, and  
162 migration of climate models has increased drastically. This has become known as the software  
163 productivity gap (Lawrence et al. 2018).

164 One important design principle of modern software engineering is the separation of concerns.  
165 It means splitting a computer program into different parts, where each part deals with a separate  
166 concern. To this end, there has been an increased interest in the development of higher-level ab-  
167 stractions for weather and climate models (Bertagna et al. 2018; Adams et al. 2019; Fuhrer et al.  
168 2014; Clement et al. 2018, e.g.,). For example, domain-specific languages (DSLs) can help sepa-  
169 rate hardware architecture-dependent details from the source code written by the climate scientists  
170 (see "Domain-specific languages explained" sidebar). As a result, the source code of a GCM or  
171 RCM implemented using a DSL is more concise and more easily maintainable.

## 172 *b. Choice of numerical methods*

173 Weather and climate models consist of a dynamical core and physical parameterizations. For  
174 large-scale atmospheric simulations at resolutions explicitly resolving deep convection, choosing  
175 a fully compressible, nonhydrostatic set of primitive equations is essential (Davies et al. 2003).

176 The optimal (fastest for a given accuracy) numerical approach for solving these equations depends  
177 on the hardware architecture and the underlying numerical method. In particular, the exchange of  
178 data across the computational mesh (and thus data movement across compute nodes) is strongly  
179 influenced by the numerical method employed. Some schemes avoid global communication (i.e.  
180 data is moved only between neighboring grid points), but have rigorous timestep restrictions (e.g.  
181 horizontally-explicit, vertically-implicit methods, see Lock et al. 2014). Others require iterative  
182 solvers and/or global communication at each timestep, but allow for much longer timesteps (e.g.  
183 semi-implicit semi-Lagrangian or pseudo-spectral methods, see Tanguay et al. 1990; Temperton  
184 et al. 2001).

185 In the real atmosphere, the speed of sound is the fastest velocity in the system. Thus, the tem-  
186 poral evolution of the atmosphere at a given location is influenced by a neighborhood determined  
187 approximately by sound propagation (Fig. 3a). This neighborhood is referred to as the physical  
188 domain of dependence. Any numerical scheme must respect this principle, and the numerical do-  
189 main of dependence must be identical to or larger than its physical counterpart. However, in order  
190 to minimize data communication, the numerical domain of dependence should also be as small as  
191 allowable. For some implementations (Zängl et al. 2015; Skamarock et al. 2012; Baldauf et al.  
192 2011; Kühnlein and Smolarkiewicz 2019) data is exchanged at about twice the minimum rate as  
193 determined by sound propagation (Fig. 3b), while the spectral approach requires global commu-  
194 nication at each time step (Fig. 3c). It is thus evident that data communication requirements are  
195 strongly affected by the underlying numerical approach, and the implied computational costs are  
196 influenced in turn by the hardware configuration of the employed supercomputer (e.g. its node-  
197 to-node network topology). With higher computational resolution (when more compute nodes  
198 become involved), or with current hardware trends (when data movement become more costly),  
199 numerical methods with little across-node communication will often have a faster performance.

200 Among other methodologies, the split-explicit approach, as employed in our work-horse  
201 COSMO model, is well suited for this challenge, as it restricts communication to near-neighbors  
202 and provides perfect weak scaling (Fuhrer et al. 2018). Perfect weak scaling means that the com-  
203 putational domain of a simulation can be expanded in parallel with the number of computational  
204 nodes employed, without increasing the wall-clock time required to run the simulation.

### 205 *c. Coping with the data avalanche*

206 The climate modeling community is already struggling to cope with the data volumes produced  
207 by the current simulation efforts. For instance, performing all the simulations considered for the  
208 Coupled Model Intercomparison Project Phase 6 (CMIP6, Eyring et al. 2016) would amount to  
209 about 800 TB of output for each of the 100 participating models (Balaji et al. 2018). While it  
210 is impossible to foresee all the experiments envisioned in future editions, projecting the output  
211 volume of the compulsory DECK simulations (Table 1) seems like an illustrative exercise. The  
212 DECK consist of four simulations, which every model participating in CMIP6 needs to complete  
213 (see Table for details). Performing these simulations at kilometer-scale resolution would exceed  
214 the expected overall data volume of CMIP6 by about three orders of magnitude (Table 1, fourth  
215 column). This assumes that only a small fraction of the total data is written to disk, while for some  
216 applications higher output frequency is needed (see, e.g., examples in Section 4c). A more recent  
217 development are DECK simulations with up to 100 – 1000 ensemble members (Large/Grand En-  
218 sembles, e.g., Maher et al. 2019). While these simulations would be particularly useful to address  
219 rare and extreme events, the expected data volume typically prevents storing data at sub-daily in-  
220 tervals, which would be essential for, e.g., the analysis of diurnal cycles, weather system dynamics,  
221 precipitation, and wind extremes.

222 One possibility to overcome the output avalanche is to merely store the simulation setup, initial  
223 conditions and restart files, and re-run the simulation on demand when needed to perform a specific  
224 analysis. A more sophisticated scheme would restart the simulation in parallel from a series of  
225 restart files. This in principle enables to arbitrarily trade off storage for computation. Depending  
226 upon the available hardware resources, an optimized design of a re-simulation (in terms of cost and  
227 time) might employ an alternate software configuration (e.g., using a different number of compute  
228 nodes), or even an alternate hardware platform.

229 In order to ensure exactly the same results when re-simulating the chaotic dynamical system,  
230 we must ensure that the simulation code itself is bitwise reproducible, i.e., produces exactly the  
231 same output, bit by bit, when re-run with the same input. Bitwise reproducibility is potentially  
232 also required across different hardware architectures, depending on the setup of the re-simulation.  
233 Whether bitwise reproducibility is required will depend upon the targeted analysis. Consider for  
234 instance an analysis focusing on a few major hurricanes in an extended simulation, then the lack of  
235 bitwise reproducibility presents a serious hurdle (as hurricanes might disappear or change with the  
236 chaotic dynamics). Alternatively, for the statistical evaluation of short-term precipitation events,  
237 bitwise reproducibility might not be needed, provided the simulation considered is sufficiently  
238 long.

239 It is often assumed that bitwise reproducibility comes at a significant performance cost. How-  
240 ever, recently, various approaches to ensure bitwise reproducibility with small performance over-  
241 heads have been demonstrated by Demmel and Nguyen (2013). Arteaga et al. (2014) demonstrated  
242 how to integrate such approaches into full scientific applications. These developments enable effi-  
243 cient re-simulation and will be discussed later in this paper.

244 *d. Compliance with Data Policies, FAIR principles*

245 In recent years the issue of data sharing and data accessibility has received growing attention  
246 (Sloan and Alper 2018; National Academies of Sciences and Medicine 2018; Schuster et al. 2019).  
247 To make maximum use and reuse of scientific data, it should be Findable, Accessible, Interoper-  
248 able und Reusable (FAIR) (Wilkinson et al. 2016). Publishers have taken action and their data  
249 policies address data accessibility. For example the American Meteorological Society (AMS) has  
250 issued a policy statement: “the AMS encourages the Earth System Science community to provide  
251 full, open, and timely access to environmental data and derived data products, as well as all associ-  
252 ated information necessary to fully understand and properly use the data (metadata)”<sup>5</sup>. Moreover,  
253 many journals require that the storage archive for the underlying data is documented in the article  
254 upon publication. Organizations such as the Coalition for Publishing Data in the Earth and Space  
255 Sciences (COPDESS) have been founded to facilitate FAIR data.

256 It is not clear yet, how the FAIR principles can be extended to include the workflow proposed  
257 in this study, namely re-simulating data once it is required for further analysis. Especially the  
258 aspect of a timely access to the data is challenging, and often the required source code is subject  
259 to some licence agreement. It is clear that these emerging strategies will also require updates of  
260 data policies. In particular, guaranteeing bitwise reproducibility over extended time periods (say  
261 5-10 years) should become a central element of the FAIR principles, as for some applications  
262 recomputation will become more cost-effective than storing the output.

---

<sup>5</sup><https://www.ametsoc.org/ams/index.cfm/about-ams/ams-statements/statements-of-the-ams-in-force/full-and-open-access-to-data/>

### 263 **3. Strategies towards km-scale resolution**

#### 264 *a. The target model*

265 In this study we use the COSMO (Consortium for Small-scale Modeling, Steppeler et al. 2003;  
266 Baldauf et al. 2011) model. COSMO is a community model used by many national weather  
267 services worldwide as well as research groups at over 100 universities. The COSMO model is a  
268 limited-area model used for both numerical weather prediction and climate modeling by the CLM-  
269 Community<sup>6</sup>. The findings and results presented in this paper have all been carried out using a  
270 version of the COSMO model refactored for heterogeneous computing architectures (Fuhrer et al.  
271 2014). This version also supports execution in single precision (Düben and Palmer 2014). The  
272 overall effort to refactor COSMO is approximately 20 man-years. We expect that the learnings  
273 presented in this article from COSMO carry over to many other models.

#### 274 *b. Domain-specific languages*

275 Dynamical cores of atmospheric or ocean models such as COSMO typically do not contain sin-  
276 gular performance hot spots that can simply be replaced with an efficient implementation<sup>7</sup>. Rather,  
277 the program code often contains a series of iterations over all grid points (for example applying  
278 a fourth order diffusion filter as in the sidebar "Domain-specific languages explained"). As men-  
279 tioned in Section 2a, achieving good performance on current high-performance computing systems  
280 requires decorating the code with hardware dependent compiler directives to specify parallelism  
281 and the schedule of how the loop iterations will be executed (see Section c). Further, optimizations  
282 often entail changes in the looping structure (e.g., blocking), the data structures, and typically also  
283 the fusion of consecutive iterations over all grid points. The consequences of the above changes

---

<sup>6</sup><https://www.clm-community.eu>

<sup>7</sup>Spectral transforms are a notable exception.

284 are loss of performance portability, significant decrease in maintainability of the code and often  
285 sub-optimal performance.

286 Choosing an alternative route, the dynamical core of the COSMO model has been rewritten using  
287 the GridTools DSL (Gysi et al. 2015; Fuhrer et al. 2014). GridTools is a domain-specific language  
288 that eases the burden of the application developer by separating the architecture dependent im-  
289 plementation strategy from the user-code. GridTools is currently implemented in C++ by using  
290 template metaprogramming; thus an application based on GridTools needs to be implemented in  
291 C++. GridTools has become publicly available under a permissive open-source license in March  
292 2019<sup>8</sup>.

### 293 *c. Use of OpenACC*

294 While code re-writing using DSLs offers many advantages in terms of performance and main-  
295 tainability, it may not be applicable to the entire code base. In addition, some parts like the physical  
296 parameterizations have been developed by a large and active community, which may not be ready  
297 for changing their programming paradigm. However, in order to avoid costly CPU to GPU data  
298 transfers, most parts of the code need to run on the GPU. To achieve this, an OpenACC compiler  
299 directive porting approach was used for all components of the COSMO model that had not been  
300 re-written using DSLs (Fuhrer et al. 2014; Lapillonne and Fuhrer 2014).

301 The OpenACC compiler directives can be added to existing code, to tell the compiler which part  
302 should run on the GPU, offering the possibility to incrementally adapt the code for GPUs. While  
303 the directive approach does not offer a hardware optimization comparable to DSLs, it allows to  
304 achieve reasonable performance. Some parts of the code have been further optimized and restruc-  
305 tured to achieve a better performance on GPUs. In some cases these changes are not performance

---

<sup>8</sup><http://www.github.com/GridTools/>

306 portable, i.e., they have a negative impact on the CPU execution time, such that two code paths  
307 – one for CPU and one for GPU – need to be maintained. Although this approach has proven  
308 successful to port large legacy codes, the OpenACC compiler directives have limitations and the  
309 long-term support of OpenACC compilers is not guaranteed at this stage. Thus our approach  
310 requires re-evaluation in the future as new programming paradigms emerge.

311 Overall the COSMO model with the re-written GridTools dynamical core and with the other  
312 components ported with OpenACC directives runs about 3 to 4 times faster on GPUs than the  
313 original code on CPUs when comparing hardware of the same generation (Fuhrer et al. 2014;  
314 Leutwyler et al. 2016). Similar speedups have been reported by other studies (Govett et al. 2017,  
315 e.g.,).

#### 316 *d. Emerging programming paradigms for climate models*

317 The complexity of climate models is already challenging at current resolutions. However, with  
318 further resolution increases, and with the need to account for newly emerging hardware architec-  
319 tures, these challenges become even more significant. In practice there is a high compartmental-  
320 ization of the model development, with dynamical cores and physics packages mostly developed  
321 in isolation (Donahue and Caldwell 2018). The immediate downside of this approach is the pro-  
322 liferation of model components with incompatible structures. Transferring such components to  
323 other models often requires a large amount of work (Randall 1996).

324 The recognition of the need for standardizing Earth system models dates back to the 1980s  
325 (Pielke and Arritt 1984). Kalnay et al. (1989) suggested a list of basic programming rules to design  
326 *plug-compatible* physics packages, enabling a high degree of scientific code exchange. This led to  
327 the idea of a common software infrastructure that couples different components while enhancing  
328 interoperability, usability, software reuse, and performance portability (Dickinson et al. 2002).



329 Notable examples of such coupling frameworks include the Earth System Modeling Framework  
330 (ESMF) combined with the National Unified Operational Prediction Capability (NUOPC) layer  
331 (Hill et al. 2004; Theurich et al. 2016), the Flexible Modeling System (FMS) (Balaji 2012), the  
332 Program for Integrated Earth System Modeling (PRISM) framework (Guilyardi et al. 2003), and  
333 the Weather Research and Forecast (WRF) code infrastructure (Michalakes et al. 2005).

334 All these frameworks are coded in Fortran, which remains the preferred programming language  
335 for software development in climate models. However, the new generations of atmospheric and  
336 computer scientists are more familiar and proficient with higher-level languages, e.g., Python.  
337 Python has been increasingly used by academics and scientists due to its clean syntax, great ex-  
338 pressiveness and a powerful ecosystem of open source packages, making it ideal for fast prototyp-  
339 ing (Millman and Aivazis 2011). Yet, its direct application in high-performance computing has  
340 historically been limited by the inherent execution slowness of the Python interpreter. Solutions to  
341 overcome the interpreter overhead exist, including DSLs endowed with lower-level and optimized  
342 backends.

343 In most of the traditional frameworks, the calling sequence of parameterizations (or components  
344 like ocean, land, and sea ice) is hard-coded for efficiency reasons. `symp1` (System for Modeling  
345 Planets; Monteiro et al. 2018) attempts to circumvent this and other limitations by providing a  
346 toolset of Python objects to build hierarchies of Earth system models, in which each component  
347 represents a physical process. A model is thus conceived as a chain of computing blocks, which  
348 act on and interact through the *state*, i.e., the set of variables describing the model state at any point  
349 in time. The state is encoded as a dictionary of multi-dimensional arrays which enables metadata-  
350 aware operations (Hoyer and Hamman 2017). To illustrate how this dictionary works, consider  
351 a scientist who intends to develop a new parameterization. In doing so, he/she requires access  
352 to specific variables of the model state. In current climate modeling frameworks, this requires

353 specific knowledge about how the data is stored and how it can be accessed. In contrast, `symp1`  
354 provides a transparent set of tools for accessing the data in the model state dictionary. The tools  
355 take care of some of the annoying issues, such as the transformation of data between different  
356 units. In doing so, it hides the complexities of the data storage in the respective parent model, and  
357 can in principle provide a general approach across many different models.

358 Currently several research groups are exploring `symp1`. In our own work, we are using it to  
359 investigate the physics time stepping. Although it appears to be of similar importance as the  
360 choice of the spatial discretization (Knoll et al. 2003), in the majority of the current weather and  
361 climate codes the time stepping is merely accurate to first order, and the results and sensitivity  
362 of models depend upon the choice of the calling sequence (e.g. Donahue and Caldwell 2018;  
363 Gross et al. 2018). It is not only the lack of a common interface, but also the simplified time  
364 stepping, that hinders the exchange of parameterizations. With the help of an idealized hydrostatic  
365 model in isentropic coordinates, we are currently conducting numerical experiments to quantify  
366 the impact of the employed coupling strategy on the solution. We find that `symp1` is a suitable  
367 prototype framework for building flexible, modular and interoperable codes, and believe that such  
368 frameworks could aid the development of future climate codes.

#### 369 *e. Bit-reproducible code*

370 A bit-reproducible climate model produces the exact same numerical results for a given preci-  
371 sion, regardless of its execution setup – which includes the choice of domain decomposition, the  
372 type of simulation (continuous or restarted), compilers, and the architectures executing the model  
373 (CPU or GPU).

374 One source of non-reproducibility stems from the way arithmetic operators are evaluated on a  
375 computer. A floating-point arithmetic operation is equivalent to the application of the operator

376 on the operands, followed by a rounding of the result:  $r(a + b) \neq a + b$ , where  $r(\cdot)$  denotes the  
377 rounding function. The latter function produces a representable floating-point value in the com-  
378 puter's memory from a real number. For simple operations (addition, subtraction, multiplication,  
379 division and square root), the IEEE-754 standard ensures bit-wise reproducibility across hard-  
380 ware architectures (Zuras et al. 2008; Arteaga et al. 2014). However, the associativity property  
381 of arithmetic operators is broken. This means that  $(a + b) + c = a + (b + c)$  is not preserved, as  
382  $r(r(a + b) + c) \neq r(a + r(b + c))$ . Although the rearrangements are equivalent in their mathematical  
383 form, they are not equal in a floating point computation.

384 Achieving reproducibility across architectures is a challenge, as compilers don't produce the  
385 same executable code when targeting different hardware architectures (i.e., GPU or CPU). Math-  
386 ematical expressions can be rewritten (contraction, re-association, fast mathematics) in different  
387 manners to ensure best performance on the targeted architecture, leading to potentially different  
388 results due to the aforementioned properties of floating-point arithmetic. The key points to achieve  
389 bit-reproducibility with COSMO are to (i) forbid the re-association of mathematical expression,  
390 (ii) forbid the creation of alternative execution strategies for a given computation, (iii) forbid the  
391 usage of mathematical approximation or contraction operators, and (iv) provide portable transcen-  
392 dental functions (i.e., logarithm, exponential function, or the trigonometric functions) to ensure  
393 reproducibility of their evaluation.

394 Compilers can be more or less aggressive with the level of optimization they apply. By using  
395 execution flags, the user can have some control over the optimizations applied during compilation.  
396 We used a set of flags that limits instructions rearrangement as much as possible (see Supple-  
397 mentary Table 1). This increases the probability that compilers targeting different architectures  
398 produce identical mathematical expressions. Finally we wrote a preprocessor to automatically  
399 add parentheses to every mathematical expressions of the model, ensuring a unique way to evalu-

400 ate these expressions. The preprocessor also replaces all intrinsic function calls with our custom  
401 version of portable transcendental functions.

402 In our work with COSMO, reproducibility between the CPU (Intel Xeon E5-2690) and GPU  
403 (Nvidia Tesla K80) versions of the model has been achieved, although at the time of writing  
404 discrepancies remain in some modules relevant for long simulations and with restarted simulations.  
405 These challenges still need to be addressed. The performance penalty of making the code bit-  
406 reproducible is acceptable (Figure 4). On the CPU the bit-reproducible version is 37% slower  
407 than the original version of the program code, and on the GPU it is 13% slower. Overall this  
408 demonstrates that the overhead associated with bit-reproducibility may be smaller than previously  
409 thought.

#### 410 *f. Virtualization layer*

411 Data produced by high-resolution simulations is expected to be potentially valuable for a large  
412 number of climate and impact scientists over the course of decades. The way this data is commonly  
413 analyzed today is by storing it on disk and letting the analysis applications access it. This solution  
414 enables the analyses to access the data with arbitrary access patterns (e.g., forward or backward  
415 in time) and guarantees that the exact same data can be re-analyzed to produce the same results.  
416 However, high-resolution simulations produce petabytes of data today, and may produce exabytes  
417 in the near future (Table 1): storing this amount of data for long periods of time is not cost-  
418 effective and, in some cases, not possible at all. This issue can be addressed by employing online  
419 (or in-situ) analyses. Online analysis provides a solution to this problem by not storing data and  
420 by coupling analyses and simulations. However, this approach leads to a loss of flexibility (e.g.,  
421 the data access pattern of the analysis must follow the the simulation), and most of the times it  
422 requires to instrument the model code with analysis software (Zhang et al. 2012) that run as the

423 data is produced by the model. While this alleviates the storage issues (for our European-scale  
424 simulations, storage for the monthly restart files amounts to only 38 GB in comparison to the  
425 standard output per month of 0.4 TB), this approach makes the analysis less flexible.

426 We developed and tested *SimFS* (Di Girolamo et al. 2019), a virtualization layer that is in be-  
427 tween the analysis applications and the simulation data (<https://github.com/spcl/SimFS>). *SimFS*  
428 exposes a virtualized view of the simulation data: the data is seen by the analysis as if it was on  
429 disk, while it may not be stored there. *SimFS* is responsible to re-create data that is being accessed  
430 by an analysis but not present on disk (i.e., on-demand).

431 Analysis applications can be transparently interfaced to the virtualization layer: calls to standard  
432 I/O libraries (e.g., netCDF, HDF5) are intercepted by a *SimFS* client library that can be loaded at  
433 runtime into the analysis application, without requiring any changes of the analysis code. To guide  
434 optimizations and gain control and information about the virtualized environment, the analysis can  
435 also interface *SimFS* through a set of specialized Application Programming Interfaces (APIs).

436 Virtualizing the simulation data means enabling the analysis of multi-petabytes datasets on ter-  
437 abytes storage systems. As a consequence, *SimFS* may need to evict data when the given storage  
438 share becomes full. To select which files to evict, *SimFS* tracks the analyses access patterns and  
439 employs caching and prefetching strategies to (1) identify the most relevant (i.e., most accessed)  
440 parts of simulation data and keep them on-disk, avoiding their resimulation and (2) minimize the  
441 time to recover missing data.

442 Figure 5 sketches the *SimFS* workflow. The scientists set up the initial simulation that runs to  
443 completion (top-left) and produces the restart files (black files in top-right) that are stored. Later,  
444 analysis tools access the simulation data through the virtualization layer (bottom-left). *SimFS*  
445 intercepts these accesses and manages/restarts simulations to recreate the requested output data if

446 not already present (bottom-right). The system can be configured to cache the simulation data on  
447 a hierarchy of data storage mediums (e.g., fast flash memories, mechanical disks, magnetic tapes).

448 SimFS requires that simulations can be restarted and deliver bitwise-identical output (see  
449 Sec. 3e). If bitwise reproducibility is not provided, analyses should be able to operate on data  
450 that can differ from the one produced by the initial simulation.

## 451 **4. Results and applications**

### 452 *a. Near-global benchmarking*

453 As stated in Section 1, there is significant thrust in the modeling community to decrease the  
454 grid spacing of global climate simulations to the kilometer-scale in order to address some of the  
455 most pressing deficiencies in understanding and projections of climate change. Fig. 1 summarizes  
456 some of the pioneering simulations that have been reported in the literature, notably the prototype  
457 simulations of Miyamoto et al. (2013) and Fuhrer et al. (2018). But how far are we from actually  
458 achieving kilometer-scale simulations on leadership class HPC facilities?

459 One of the most important metrics for assessing the usability of climate simulations is the simu-  
460 lation throughput measured in simulated years per wall-clock day (SYPD). Different applications  
461 of global climate models require different minimal simulation throughput in order to be feasible.  
462 For example, a global climate model achieving 1 SYPD on a given HPC system can be considered  
463 useful for simulations spanning several decades. While not sufficient for all applications, 1 SYPD  
464 can be considered a reasonable first target for global kilometer-scale climate simulations.

465 Since COSMO is one of the few models which has been systematically adapted to run on modern  
466 supercomputer architectures with GPU-accelerated node designs, it is an interesting benchmark to  
467 consider. Fuhrer et al. (2018) report a simulation throughput of 0.043 SYPD for idealized, near-

468 global simulations using the COSMO model on 4,888 nodes of the Piz Daint supercomputer at  
469 CSCS with a grid spacing of 0.93 km. In an detailed analysis, Schulthess et al. (2018) conclude,  
470 that this result corresponds to an approximately 100x shortfall with respect to the defined goal.

471 Summit, the system currently leading the TOP500 ranking of supercomputers, has approxi-  
472 mately 5x more GPUs than Piz Daint and a more recent generation of GPUs (NVIDIA Tesla  
473 V100 16GB) which execute COSMO 1.5x faster than the GPUs in Piz Daint (NVIDIA Tesla P100  
474 16GB). We can not expect to be able to scale COSMO to the full Summit system, but results  
475 from Fuhrer et al. (2018) indicate that further linear strong scalability by a factor three is possible.  
476 Taking these factors into account, we find that running a global climate simulation with a realistic  
477 setup (cf. Table 1 of Schulthess et al. 2018) and a horizontal grid spacing of 1 km on the currently  
478 largest supercomputer available would fall short of the 1 SYPD target by approximately a factor  
479 of 20x (Schulthess et al. 2018). A recent study by Neumann et al. (2019) reports a shortfall of  
480 a factor of 30x, extrapolating results from the ICON model at 5 km grid spacing and assuming  
481 perfect weak scaling.

482 Addressing the remaining shortfall will likely require a combination of several strategies, in-  
483 cluding algorithmic, software and hardware improvements. Addressing the challenge of I/O for  
484 global kilometer-scale simulations will require fundamental changes in our simulation and analy-  
485 sis workflow such as SimFS.

486 However, at a resolution of 2 km, the simulation throughput of COSMO on Piz Daint for a  
487 regional climate simulation setup already reaches 0.23 SYPD, thus the model can already be used  
488 for decade-long continental-scale simulations at such a resolution. Some examples are shown in  
489 the next section.

490 *b. Regional climate simulations*

491 There are three areas where km-scale resolution is raising hopes for significant benefits. First,  
492 there is a better representation of the underlying surface – complex topography, coast lines, and  
493 land-surface properties. Second, higher resolution allows to better represent meso-scale pro-  
494 cesses and the associated feedbacks to the larger scale, such as fronts, orographic wind systems,  
495 boundary-layer processes, and soil-moisture atmosphere feedbacks. Third, and likely most impor-  
496 tantly, km-scale resolution allows switching off two of the most critical parameterizations in cli-  
497 mate models, namely moist convection and gravity-wave drag, which constitute critical sources of  
498 uncertainties in climate change projections. Explicit simulation of convection has led to significant  
499 improvements in simulations of the diurnal cycle of precipitation, addressing aspects of frequency  
500 and intensity of heavy hourly precipitation (e.g., Kendon et al. 2012; Ban et al. 2014, 2015; Prein  
501 et al. 2015; Leutwyler et al. 2017; Berthou et al. 2018), which can potentially lead to hydrological  
502 impacts like flash floods, floods and landslides. An example of this is shown in Figure 6 for hourly  
503 precipitation over Europe on a summer day. The 12 km model produces widespread low-intensity  
504 precipitation (a long-standing problem of convective parameterizations), while a more realistic  
505 representation of intense summer precipitation is obtained in the 2 km model. Furthermore, km-  
506 scale resolution is needed for resolving local scale wind systems, like sea breeze and orographic  
507 circulations (e.g., Belušić et al. 2018), and for a better representation of clouds and their vertical  
508 profiles (e.g., Hentgen et al. 2019).

509 A comparison of cloud cover at different resolutions over the tropical Atlantic is shown in Fig-  
510 ure 7. In comparison with MODIS<sup>9</sup> (Moderate Resolution Imaging Spectroradiometer imagery)  
511 observations, convection-parameterized simulations at 50 and 12 km show an overestimation of  
512 clouds and do not reproduce the organized cloud structures visible in observations. In contrast,

---

<sup>9</sup><https://terra.nasa.gov/about/terra-instruments/modis>



513 the 2 km simulation with explicit convection can qualitatively reproduce the characteristic cloud  
514 structures known as mesoscale cloud flowers (e.g., Bony et al. 2017). More detailed analysis  
515 demonstrates that the use of explicit convection also significantly reduces top-of-the-atmosphere  
516 radiation biases. The simulations suggest that the organization of the subtropical clouds considered  
517 does not overly depend upon small-scale processes truncated at km-scale resolution. Animations  
518 of these simulations are shown in the Electronic Supplement.

519 In addition to a better representation of the present-day climate, convection-resolving climate  
520 models provide modified climate change signals. Although changes in mean seasonal precipi-  
521 tation are generally robust between convection-resolving and convection-parameterizing models,  
522 significant differences occur for projections of heavy hourly precipitation events (Ban et al. 2015;  
523 Kendon et al. 2017) and for changes in the vertical structure of clouds (Hentgen et al. 2019).

524 Convection-resolving and convection-parameterizing models often exhibit important differences  
525 for sub-daily variables, or when feedback effects are considered. Most of the analysis in current  
526 climate studies is done using two-dimensional daily and/or hourly output fields, which are cur-  
527 rently feasible to store. Three-dimensional fields are usually not available over extended time  
528 periods, which limits detailed investigations of the flow dynamics. Convective clouds can grow,  
529 mature and dissipate within an hour, and thus it is difficult to gain deeper understanding of con-  
530 vection and its characteristics in current and future climates if restricted to hourly output fields.

531 Refining the horizontal resolution of regional climate models is a key focus in a number of  
532 internationally coordinated projects, like CORDEX<sup>10</sup> and EUCP<sup>11</sup>. Within these two projects,  
533 several groups across Europe are conducting regional climate simulations in common domains  
534 with horizontal resolutions around 3 km, with the aim of producing a multi-model ensemble of

---

<sup>10</sup>COordinated Regional Downscaling EXperiment, <http://www.cordex.org>

<sup>11</sup>European Climate Prediction System, <https://www.eucp-project.eu>

535 climate simulations (Coppola et al. 2018). Similar initiatives are also underway within GEWEX<sup>12</sup>.  
536 The availability of long-term high-resolution simulations would also enable to link to short-term  
537 case studies (e.g. Dauhut et al. 2015) and idealized simulations of convective events (e.g. Loriaux  
538 et al. 2017).

539 *c. Sophisticated analysis using the virtualization layer*

540 This section presents online analysis applications of convection-resolving COSMO simulations  
541 with SimFS, and briefly discusses the limitations of offline and online analyses. An offline analysis  
542 would follow the traditional approach of saving all necessary fields on disk (e.g., with a temporal  
543 resolution of 1 h) and then running the diagnostic. In contrast, an online analysis would be run as  
544 part of the main model forward integration, allowing for an almost arbitrary temporal resolution  
545 of input fields – e.g., online forward trajectory calculations (Miltenberger et al. 2016). In the  
546 following, two applications are considered, with differing requirements in terms of the temporal  
547 resolution and data volume of the input fields. The results are based on a week-long COSMO  
548 simulation, starting at 00 UTC 10 April 2000. The first application tracks precipitation cells, and  
549 the second uses backward trajectories to investigate the Foehn flow in an Alpine valley.

550 Precipitation cells are identified every 6 min using a threshold of  $2 \text{ mm h}^{-1}$  and tracked in time  
551 with a criterion considering feature overlap and size (Rüdisühli 2018). Access to the data is pro-  
552 vided through SimFS, i.e. without storing it on disk. In order to speed up the analysis, the grid  
553 resolution is reduced by averaging the surface precipitation field over  $3 \times 3$  grid points, and a min-  
554 imum feature size of two coarse grid points is required. To facilitate the tracking, the overlap  
555 of features in consecutive steps is increased temporarily by 3 coarse grid points in all directions.  
556 Results are shown in Figure 8. At 10 UTC 12 April 2000, precipitation occurs over large areas,

---

<sup>12</sup><https://ral.ucar.edu/events/2018/cpcm>

557 extending along a frontal band extending from the British Isles over Germany to the Alps, and  
558 in the form of small shower cells in the Bay of Biscay and adjacent regions (Figure 8a). The  
559 cell tracking reveals the strongly differing lifetimes of the various cells, ranging from minutes to  
560 days (Figure 8b). While short-lived cells produce less precipitation than longer-lived cells, they  
561 are more frequent. An animation of this figure over an extended period is provided in the Elec-  
562 tronic Supplement. SimFS allows to use this approach for tracking precipitation cells at temporal  
563 resolutions of a few minutes in long climate simulations without storing the fields on disk.

564 The second application is based on air-parcel trajectories, which implies considerable compu-  
565 tational challenges for SimFS: The trajectories are run 12 h backward in time and hence do not  
566 follow the forward integration of the COSMO simulation (backward trajectories prohibit a stan-  
567 dard online implementation). The trajectories are released in a narrow (2-5 km wide) Alpine valley  
568 and therefore the temporal resolution of the wind fields must be high in order to capture the spatial  
569 and temporal variability of the winds as the air parcels descend into the valley. The backward tra-  
570 jectories are initialized in the upper Rhine valley – a classical Alpine Foehn valley (e.g., Würsch  
571 and Sprenger 2015) (see Supplementary Figure 1). Trajectory computations use wind fields at  
572 different update intervals from 1 to 60 min. Results show that depending upon the case, there is  
573 considerable sensitivity to the temporal resolution, pinpointing different origins of the air parcels.  
574 This illustrates the importance of using input fields with very high temporal resolution (1 to 5 min).  
575 This example further emphasizes the value of SimFS: it allows computing backward trajectories  
576 (which would be difficult with a standard online implementation) with winds at very high temporal  
577 resolution (which would not be possible with an offline implementation).

578 The two applications differ substantially in terms of their computational requirements. For the  
579 Foehn flow the bottleneck is I/O, due to the demand of 3D wind fields at high temporal resolution.  
580 The calculation of the trajectories is then rather cheap. In contrast, the precipitation cell track-

581 ing relies on 2D fields only. Therefore, it is not restricted by I/O but rather by the cell tracking  
582 algorithm itself. Both requirements are relevant when using SimFS to analyze long climate simu-  
583 lations. SimFS provides a lot of flexibility. For instance, an analysis may be designed conditional  
584 upon the occurrence of a particular weather event, such as the occurrence of a hurricane or in our  
585 example the occurrence of Foehn flow at a particular location.

## 586 **5. Conclusions and Outlook**

587 In this article we have explored the use of a high-resolution modeling system for extended simu-  
588 lations over a large computational domain, and discussed potential challenges associated with the  
589 further development of climate models. A series of fundamental technology transitions are having  
590 a profound impact on the development of models, simulation software, and modeling workflows:

- 591 1. Moving data has increasingly become more expensive than arithmetic operations. While in  
592 the past compute performance has commonly been expressed in floating point operations  
593 per second, the energy and runtime footprints of high-resolution atmospheric models are  
594 dominated by accessing system memory.
- 595 2. Energy costs of large compute centers have increased by a factor of 10-20 relative to hardware  
596 costs over the last two decades (Schulthess et al. 2018) and are increasingly affecting the  
597 design and implementation strategies of major supercomputing centers.
- 598 3. While early supercomputers used chips that were specifically designed for science applica-  
599 tions, today's supercomputers are commonly based on commodity hardware that is produced  
600 in large quantities for a wide range of markets.
- 601 4. The common climate-modeling workflow – i.e., run the model on a supercomputer, store the  
602 results on a mass-storage system, and run analysis software on the stored results – increas-

603 ingly approaches a bottleneck. The bandwidth of mass-storage systems does not keep up with  
604 the speed at which high-resolution models produce data, and the cost of storage increases  
605 faster than that of compute power.

606 The high cost of data movement favors hardware architectures with deep memory hierarchies  
607 having multiple layers of cache that have to be managed explicitly. Further, power constraints  
608 lead to heterogeneous node designs where accelerators such as graphics processing units deliver  
609 the bulk of the compute capacity. Current atmospheric models are unable to fully exploit such  
610 hardware. One hindrance are currently-used programming languages, which impose the burden of  
611 leveraging the hardware architecture on the model developer.

612 In this article we have used the limited-area model COSMO and have explored a range of options  
613 to address these challenges. In particular, we have:

- 614 ● further developed and used a model version that uses the domain-specific language (DSL)  
615 GridTools. These languages enable a high-level abstraction to stencil operations and allow  
616 for a separation of concerns, i.e., the model source code is less contaminated by hardware-  
617 specific implementation details and optimizations.
- 618 ● developed and tested a novel modeling workflow that is based on recomputation and online  
619 analyses (rather than storing the results). This exploits a virtualization environment (SimFS),  
620 which transparently provides data access in a similar fashion as used today for the analysis of  
621 climate data on mass-storage systems.
- 622 ● explored a bit-reproducible version of the model code, to enable bit-wise reproducible simu-  
623 lations across two different hardware architectures and different compilers.
- 624 ● tested new programming paradigms such as the SYMPL framework to ease the work with  
625 complex codes and parameterizations in a Python environment.

626 Some of the new developments (the GPU-enabled COSMO model) have been used operationally  
627 at MeteoSwiss for several years, others (i.e. SimFS) have been developed and tested in extended  
628 regional climate model integrations, and still others will require further development before be-  
629 coming applicable in full climate simulations (e.g. the use of SYMPL and bit-reproducible code  
630 versions). Results demonstrate the functionality of the approach, and also provide a look into  
631 future capabilities of climate models at high spatial resolution.

632 We discussed our experience with COSMO as background material for future model devel-  
633 opments, but we are aware that additional challenges will emerge if applied to other numerical  
634 approaches and to global model applications. It is worth mentioning that the GridTools DSL is  
635 currently being extended for applications with some global meshes. However, we have not yet  
636 started to work on addressing the complexities of efficiently coupling atmosphere and ocean mod-  
637 els in full-blown earth system models.

638 *Acknowledgments.* Some of this work was supported by the Swiss National Science Foundation  
639 under Sinergia grant CRSII2 154486/1 crCLIM, and several projects under the Swiss Platform for  
640 Advanced Scientific Computing (PASC). In addition we acknowledge PRACE for awarding us  
641 access to Piz Daint at CSCS, Switzerland. To estimate the current and future CMIP data volume  
642 in Table 1, version 01.00.28 of the Data Request Python API written by Martin Juckes from the  
643 Centre for Environmental Data Analysis (CEDA) has been used. Additional input and suggestions  
644 on the topic have been provided by a number of individuals, among these Peter Düben, Carlos  
645 Osuna, Bjorn Stevens, Pier Luigi Vidale, and 2 anonymous referees.

## 646 **References**

647 Adams, S. V., and Coauthors, 2019: Lfric: Meeting the challenges of scalability and performance  
648 portability in weather and climate models. *J. Parallel Distr. Com.*

- 649 Arteaga, A., O. Fuhrer, and T. Hoefler, 2014: Designing bit-reproducible portable high-  
650 performance applications. *Proc. of the 28th IEEE Int. Parallel and Distributed Processing Symp.*  
651 (*IPDPS*), IEEE Computer Society.
- 652 Balaji, V., 2012: The flexible modeling system. *Earth system modelling-volume 3*, Springer, 33–  
653 41.
- 654 Balaji, V., and Coauthors, 2018: Requirements for a global data infrastructure in support of cmip6.  
655 *Geosc. Mod. Dev.*, **11** (9), 3659–3680.
- 656 Baldauf, M., A. Seifert, J. Förstner, D. Majewski, M. Raschendorfer, and T. Reinhardt, 2011:  
657 Operational convective-scale numerical weather prediction with the cosmo model: description  
658 and sensitivities. *Mon. Wea. Rev.*, **139** (12), 3887–3905.
- 659 Ban, N., J. Schmidli, and C. Schär, 2014: Evaluation of the convection-resolving regional climate  
660 modeling approach in decade-long simulations. *J. Geophys. Res.-Atmos.*, **119** (13), 7889–7907.
- 661 Ban, N., J. Schmidli, and C. Schär, 2015: Heavy precipitation in a changing climate: Does short-  
662 term summer precipitation increase faster? *Geophys. Res. Lett.*, **42** (4), 1165–1172.
- 663 Belušić, A., M. T. Prtenjak, I. Güttler, N. Ban, D. Leutwyler, and C. Schär, 2018: Near-surface  
664 wind variability over the broader adriatic region: insights from an ensemble of regional climate  
665 models. *Clim. Dyn.*, **50** (11-12), 4455–4480.
- 666 Bertagna, L., M. Deakin, O. Guba, D. Sunderland, A. M. Bradley, I. K. Tezaur, M. A. Taylor,  
667 and A. G. Salinger, 2018: Hommexx 1.0: A performance portable atmospheric dynamical core  
668 for the energy exascale earth system model. Tech. rep., Sandia National Lab.(SNL-NM), Albu-  
669 querque, NM (United States); Sandia . . . .

670 Berthou, S., E. J. Kendon, S. C. Chan, N. Ban, D. Leutwyler, C. Schär, and G. Fosser, 2018: Pan-  
671 european climate at convection-permitting scale: a model intercomparison study. *Clim. Dyn.*,  
672 1–25.

673 Bony, S., and J.-L. Dufresne, 2005: Marine boundary layer clouds at the heart of tropical cloud  
674 feedback uncertainties in climate models. *Geophys. Res. Lett.*, **32** (20).

675 Bony, S., and Coauthors, 2017: Eurec 4 a: a field campaign to elucidate the couplings between  
676 clouds, convection and circulation. *Surv. Geophys.*, **38** (6), 1529–1568.

677 Bretherton, C. S., and M. F. Khairoutdinov, 2015: Convective self-aggregation feedbacks in near-  
678 global cloud-resolving simulations of an aquaplanet. *J. Adv. Model. Earth Syst.*, **7** (4), 1765–  
679 1787.

680 CEDA, 2018: CMIP6 data request. Centre for Environmental Data Analysis (CEDA), accessed:  
681 2018-11-19, [http://clipc-services.ceda.ac.uk/dreq/tab01\\_1\\_1.html](http://clipc-services.ceda.ac.uk/dreq/tab01_1_1.html).

682 Charney, J. G., and Coauthors, 1979: *Carbon dioxide and climate: a scientific assessment*. Natl.  
683 Acad. Sci.

684 Clement, V., S. Ferrachat, O. Fuhrer, X. Lapillonne, C. E. Osuna, R. Pincus, J. Rood, and  
685 W. Sawyer, 2018: The claw dsl: Abstractions for performance portable weather and climate  
686 models. *Proceedings of the Platform for Advanced Scientific Computing Conference*, ACM, 2.

687 Coppola, E., and Coauthors, 2018: A first-of-its-kind multi-model convection permitting ensemble  
688 for investigating convective phenomena over europe and the mediterranean. *Clim. Dyn.*, 1–32.

689 Dauhut, T., J. P. Chaboureau, J. Escobar, and P. Mascart, 2015: Large-eddy simulations of Hector  
690 the convector making the stratosphere wetter. *Atmos. Sci. Lett.*, **16**, doi:10.1002/asl2.534.



- 691 Davies, T., A. Staniforth, N. Wood, and J. Thuburn, 2003: Validity of anelastic and other equation  
692 sets as inferred from normal-mode analysis. *Quart. J. Roy. Meteor. Soc.*, **129** (593), 2761–2775.
- 693 Demmel, J., and H. D. Nguyen, 2013: Fast reproducible floating-point summation. *2013 IEEE*  
694 *21st Symposium on Computer Arithmetic*, 163–172.
- 695 Di Girolamo, S., P. Schmid, T. Schulthess, and T. Hoefler, 2019: Simfs: A simulation data vir-  
696 tualizing file system interface. *Accepted at the 33rd IEEE International Parallel & Distributed*  
697 *Processing Symposium (IPDPS'19)*, IEEE.
- 698 Dickinson, R. E., and Coauthors, 2002: How can we advance our weather and climate models as  
699 a community? *Bull. Amer. Meteor. Soc.*, **83** (3), 431–436.
- 700 Donahue, A. S., and P. M. Caldwell, 2018: Impact of physics parameterization ordering in a global  
701 atmosphere model. *J. Adv. Mod. Earth Syst.*, **10** (2), 481–499.
- 702 Düben, P. D., and T. Palmer, 2014: Benchmark tests for numerical weather forecasts on inexact  
703 hardware. *Mon. Wea. Rev.*, **142** (10), 3809–3829.
- 704 Eyring, V., S. Bony, G. A. Meehl, C. A. Senior, B. Stevens, R. J. Stouffer, and K. E. Taylor, 2016:  
705 Overview of the coupled model intercomparison project phase 6 (cmip6) experimental design  
706 and organization. *Geosc. Mod. Dev.*, **9**.
- 707 Fuhrer, O., C. Osuna, X. Lapillonne, T. Gysi, B. Cumming, M. Bianco, A. Arteaga, and T. C.  
708 Schulthess, 2014: Towards a performance portable, architecture agnostic implementation strat-  
709 egy for weather and climate models. *Supercomputing frontiers and innovations*, **1** (1), 45–62.
- 710 Fuhrer, O., and Coauthors, 2018: Near-global climate simulation at 1 km resolution: establishing  
711 a performance baseline on 4888 gpus with cosmo 5.0. *Geosc. Mod. Dev.*, **11** (4), 1665–1681.

- 712 Govett, M., and Coauthors, 2017: Parallelization and performance of the nim weather model on  
713 cpu, gpu, and mic processors. *Bull. Amer. Meteor. Soc.*, **98** (10), 2201–2213.
- 714 Gregory, J. M., R. Stouffer, S. Raper, P. Stott, and N. Rayner, 2002: An observationally based  
715 estimate of the climate sensitivity. *J. Clim.*, **15** (22), 3117–3121.
- 716 Gross, M., and Coauthors, 2018: Physics–dynamics coupling in weather, climate, and earth system  
717 models: challenges and recent progress. *Mon. Wea. Rev.*, **146** (11), 3505–3544.
- 718 Guilyardi, E., R. Budich, G. Komen, and G. Brasseur, 2003: PRISM system specification hand-  
719 book, version 1. *PRISM report series*, 230.
- 720 Gysi, T., C. Osuna, O. Fuhrer, M. Bianco, and T. C. Schulthess, 2015: Stella: A domain-specific  
721 tool for structured grid methods in weather and climate models. *Proceedings of the International*  
722 *Conference for High Performance Computing, Networking, Storage and Analysis*, ACM, 41.
- 723 Haarsma, R. J., and Coauthors, 2016: High resolution model intercomparison project (highresmip  
724 v1. 0) for cmip6. *Geosc. Mod. Dev.*, **9** (11), 4185–4208.
- 725 Harvey, B., J. Methven, C. Eagle, and H. Lean, 2017: Does the representation of flow structure  
726 and turbulence at a cold front converge on multiscale observations with model resolution? *Mon.*  
727 *Wea. Rev.*, **145** (11), 4345–4363.
- 728 Hentgen, L., N. Ban, L. D. Kröner, Nico, and C. Schär, 2019: Clouds in convection resolving  
729 climate simulations over Europe. *J. Geophys. Res. – Atmos.*, **124**, 3849–3870, doi:10.1029/  
730 2018JD030150.
- 731 Hewitt, H. T., and Coauthors, 2017: Will high-resolution global ocean models benefit coupled  
732 predictions on short-range to climate timescales? *Ocean Model.*, **120**, 120–136.

733 Hill, C., C. DeLuca, V. Balaji, M. Suarez, and A. d. Silva, 2004: The architecture of the earth  
734 system modeling framework. *Comput. Sci. Eng.*, **6** (1), 18–28.

735 Hoyer, S., and J. Hamman, 2017: xarray: Nd labeled arrays and datasets in python. *Journal of*  
736 *Open Research Software*, **5** (1).

737 IPCC, 1995: Climate change 1995: The science of climate change. Cambridge University Press,  
738 586 pp.

739 IPCC, 2001: Climate change 2001: The scientific basis. Cambridge University Press, 881 pp.

740 IPCC, 2013: Climate change 2013: The physical science basis. Cambridge University Press, 1535  
741 pp.

742 Ito, J., S. Hayashi, A. Hashimoto, H. Ohtake, F. Uno, H. Yoshimura, T. Kato, and Y. Yamada,  
743 2017: Stalled improvement in a numerical weather prediction model as horizontal resolution  
744 increases to the sub-kilometer scale. *SOLA*, **13**, 151–156.

745 Juckes, M., V. Eyring, K. Taylor, V. Balaji, and R. Stouffer, 2015: The CMIP6 Data Request: the  
746 next generation climate archive. *EGU General Assembly Conference Abstracts*, EGU General  
747 Assembly Conference Abstracts, Vol. 17, 13112.

748 Kalnay, E., and Coauthors, 1989: Rules for interchange of physical parameterizations. *Bull. Amer.*  
749 *Meteor. Soc.*, **70** (6), 620–622.

750 Kendon, E. J., N. M. Roberts, H. J. Fowler, M. J. Roberts, S. C. Chan, and C. A. Senior, 2014:  
751 Heavier summer downpours with climate change revealed by weather forecast resolution model.  
752 *Nature Climate Change*, **4** (7), 570.

753 Kendon, E. J., N. M. Roberts, C. A. Senior, and M. J. Roberts, 2012: Realism of rainfall in a very  
754 high-resolution regional climate model. *J. Clim.*, **25** (17), 5791–5806.

- 755 Kendon, E. J., and Coauthors, 2017: Do convection-permitting regional climate models improve  
756 projections of future precipitation change? *Bull. Amer. Meteor. Soc.*, **98** (1), 79–93.
- 757 Kestor, G., R. Gioiosa, D. J. Kerbyson, and A. Hoisie, 2013: Quantifying the energy cost of data  
758 movement in scientific applications. *2013 IEEE international symposium on workload charac-*  
759 *terization (IISWC)*, IEEE, 56–65.
- 760 Knoll, D., L. Chacon, L. Margolin, and V. Mousseau, 2003: On balanced approximations for time  
761 integration of multiple time scale systems. *J. Comput. Phys.*, **185** (2), 583–611.
- 762 Knote, C., G. Heinemann, and B. Rockel, 2010: Changes in weather extremes: Assessment of  
763 return values using high-resolution climate simulations at convection-resolving scale. *Meteor.*  
764 *Z.*, **19**, 11–23.
- 765 Kühnlein, C., and P. K. Smolarkiewicz, 2019: A nonhydrostatic finite-volume option for the ifs.  
766 *ECMWF Newsletter*, **158**, 30–36.
- 767 Langhans, W., J. Schmidli, and C. Schär, 2012: Bulk convergence of cloud-resolving simulations  
768 of moist convection over complex terrain. *J. Atmos. Sci.*, **69** (7), 2207–2228.
- 769 Lapillonne, X., and O. Fuhrer, 2014: Using compiler directives to port large scientific applications  
770 to gpus: An example from atmospheric science. *Parallel Process. Lett.*, **24** (01), 1450 003.
- 771 Lawrence, B. N., and Coauthors, 2018: Crossing the chasm: how to develop weather and climate  
772 models for next generation computers? *Geosc. Mod. Dev.*, **11**, 1799–1821.
- 773 Leutwyler, D., O. Fuhrer, X. Lapillonne, D. Lüthi, and C. Schär, 2016: Towards european-scale  
774 convection-resolving climate simulations with gpus: a study with cosmo 4.19. *Geosc. Mod.*  
775 *Dev.*, **9** (9), 3393–3412.

- 776 Leutwyler, D., D. Lüthi, N. Ban, O. Fuhrer, and C. Schär, 2017: Evaluation of the convection-  
777 resolving climate modeling approach on continental scales. *J. Geophys. Res.-Atmos.*, **122** (10),  
778 5237–5258.
- 779 Liu, C., and Coauthors, 2017: Continental-scale convection-permitting modeling of the current  
780 and future climate of north america. *Clim. Dyn.*, **49** (1-2), 71–95.
- 781 Lock, S.-J., N. Wood, and H. Weller, 2014: Numerical analyses of runge–kutta implicit–explicit  
782 schemes for horizontally explicit, vertically implicit solutions of atmospheric models. *Quart. J.*  
783 *Roy. Meteor. Soc.*, **140** (682), 1654–1669.
- 784 Loriaux, J. M., G. Lenderink, and A. P. Siebesma, 2017: Large-scale controls on extreme precipi-  
785 tation. *J. Clim.*, **30** (3), 955–968, doi:10.1175/JCLI-D-16-0381.1.
- 786 Maher, N., and Coauthors, 2019: The max planck institute grand ensemble-enabling the explo-  
787 ration of climate system variability. *J. Adv. Model. Earth Syst.*
- 788 Michalakes, J., J. Dudhia, D. Gill, T. Henderson, J. Klemp, W. Skamarock, and W. Wang, 2005:  
789 The weather research and forecast model: software architecture and performance. *Use of High*  
790 *Performance Computing in Meteorology*, World Scientific, 156–168.
- 791 Millman, K. J., and M. Aivazis, 2011: Python for scientists and engineers. *Comput. Sci. Eng.*,  
792 **13** (2), 9–12.
- 793 Miltenberger, A. K., S. Reynolds, and M. Sprenger, 2016: Revisiting the latent heating contribu-  
794 tion to foehn warming: Lagrangian analysis of two foehn events over the swiss alps. *Quart. J.*  
795 *Roy. Meteor. Soc.*, **142** (698), 2194–2204.

- 796 Miyamoto, Y., Y. Kajikawa, R. Yoshida, T. Yamaura, H. Yashiro, and H. Tomita, 2013: Deep  
797 moist atmospheric convection in a subkilometer global simulation. *Geophys. Res. Lett.*, **40** (18),  
798 4922–4926.
- 799 Molka, D., D. Hackenberg, R. Schöne, and M. S. Müller, 2010: Characterizing the energy con-  
800 sumption of data transfers and arithmetic operations on x86-64 processors. *International con-  
801 ference on green computing*, IEEE, 123–133.
- 802 Monteiro, J. M., J. McGibbon, and R. Caballero, 2018: `symp1` (v. 0.4.0) and `climt` (v. 0.15.3) –  
803 towards a flexible framework for building model hierarchies in Python. *Geosc. Mod. Dev.*, **11**,  
804 3781–3794.
- 805 National Academies of Sciences, E., and Medicine, 2018: *International Coordination for Sci-  
806 ence Data Infrastructure: Proceedings of a Workshop—in Brief*. The National Academies Press,  
807 Washington, DC, doi:10.17226/25015.
- 808 Neumann, P., and Coauthors, 2019: Assessing the scales in numerical weather and climate pre-  
809 dictions: will exascale be the rescue? *Philosophical Transactions of the Royal Society A*,  
810 **377** (2142), 20180148.
- 811 Palmer, T., 2014: Climate forecasting: build high-resolution global climate models. *Nature News*,  
812 **515** (7527), 338.
- 813 Panosetti, D., L. Schlemmer, and C. Schär, 2018: Convergence behavior of idealized convection-  
814 resolving simulations of summertime deep moist convection over land. *Clim. Dyn.*, doi:10.1007/  
815 s00382-018-4229-9.

- 816 Panosetti, D., L. Schlemmer, and C. Schär, 2019: Bulk and structural convergence at convection-  
817 resolving scales in real-case simulations of summertime moist convection over land. *Quart. J.*  
818 *Roy. Meteor. Soc.*, **145 (721)**, 1427–1443, doi:10.1002/qj.3502.
- 819 Pielke, R. A., and R. W. Arritt, 1984: A proposal to standardize models. *Bull. Amer. Meteor. Soc.*,  
820 **65 (10)**, 1082–1082.
- 821 Prein, A. F., R. M. Rasmussen, K. Ikeda, C. Liu, M. P. Clark, and G. J. Holland, 2017: The future  
822 intensification of hourly precipitation extremes. *Nature Climate Change*, **7 (1)**, 48.
- 823 Prein, A. F., and Coauthors, 2015: A review on regional convection-permitting climate modeling:  
824 Demonstrations, prospects, and challenges. *Rev. Geophys.*, **53 (2)**, 323–361.
- 825 Randall, D. A., 1996: A university perspective on global climate modeling. *Bull. Amer. Meteor.*  
826 *Soc.*, **77 (11)**, 2685–2690.
- 827 Ringler, T., M. Petersen, R. L. Higdon, D. Jacobsen, P. W. Jones, and M. Maltrud, 2013: A multi-  
828 resolution approach to global ocean modeling. *Ocean Model.*, **69**, 211–232.
- 829 Rüdīsühli, S., 2018: Attribution of rain to cyclones and fronts over Europe in a kilometer-scale  
830 regional climate simulation. Ph.D. thesis, ETH Zurich.
- 831 Sakamoto, T. T., and Coauthors, 2012: Miroc4h—a new high-resolution atmosphere-ocean cou-  
832 pled general circulation model. *J. Meteor. Soc. Japan*, **90 (3)**, 325–359.
- 833 Satoh, M., B. Stevens, F. Judt, M. Khairoutdinov, S.-J. Lin, W. M. Putman, and P. Düben, 2019:  
834 Global cloud-resolving models. *Current Climate Change Reports*.
- 835 Schneider, T., C. M. Kaul, and K. G. Pressel, 2019: Possible climate transitions from breakup of  
836 stratocumulus decks under greenhouse warming. *Nature Geosc.*, **12 (3)**, 163.

- 837 Schneider, T., J. Teixeira, C. Bretherton, F. Brient, K. Pressel, C. Schär, and A. Siebesma, 2017:  
838 Climate goals and computing the future of clouds. *Nat. Clim. Chang.*, **7**, 3–5.
- 839 Schulthess, T. C., P. Bauer, N. Wedi, O. Fuhrer, T. Hoefler, and C. Schär, 2018: Reflecting on the  
840 goal and baseline for exascale computing: A roadmap based on weather and climate simulations.  
841 *Comput. Sci. Eng.*, **21 (1)**, 30–41.
- 842 Schuster, D. C., and Coauthors, 2019: Challenges and future directions for data management in  
843 the geosciences. *Bull. Amer. Meteor. Soc.*, **100 (5)**, 909–912.
- 844 Sherwood, S. C., S. Bony, and J.-L. Dufresne, 2014: Spread in model climate sensitivity traced to  
845 atmospheric convective mixing. *Nature*, **505 (7481)**, 37.
- 846 Skamarock, W. C., 2004: Evaluating mesoscale nwp models using kinetic energy spectra. *Mon.*  
847 *Wea. Rev.*, **132 (12)**, 3019–3032.
- 848 Skamarock, W. C., J. B. Klemp, M. G. Duda, L. D. Fowler, S.-H. Park, and T. D. Ringler, 2012: A  
849 multiscale nonhydrostatic atmospheric model using centroidal voronoi tessellations and c-grid  
850 staggering. *Mon. Wea. Rev.*, **140 (9)**, 3090–3105.
- 851 Sloan, S. S., and J. Alper, Eds., 2018: *Data Matters: Ethics, Data, and International Research*  
852 *Collaboration in a Changing World: Proceedings of a Workshop*. The National Academies  
853 Press, Washington, DC, doi:10.17226/25214.
- 854 Steppeler, J., G. Doms, U. Schättler, H. Bitzer, A. Gassmann, U. Damrath, and G. Gregoric, 2003:  
855 Meso-gamma scale forecasts using the nonhydrostatic model lm. *Meteor. Atmos. Phys.*, **82 (1-4)**,  
856 75–96.
- 857 Tanguay, M., A. Robert, and R. Laprise, 1990: A semi-implicit semi-lagrangian fully compressible  
858 regional forecast model. *Mon. Wea. Rev.*, **118 (10)**, 1970–1980.



- 859 Temperton, C., M. Hortal, and A. Simmons, 2001: A two-time-level semi-lagrangian global spec-  
860 tral model. *Quart. J. Roy. Meteor. Soc.*, **127** (571), 111–127.
- 861 Theurich, G., and Coauthors, 2016: The earth system prediction suite: toward a coordinated us  
862 modeling capability. *Bull. Amer. Meteor. Soc.*, **97** (7), 1229–1247.
- 863 Wilkinson, M. D., and Coauthors, 2016: The fair guiding principles for scientific data management  
864 and stewardship. *Sci Data*, **3**.
- 865 Würsch, M., and M. Sprenger, 2015: Swiss and austrian foehn revisited: a lagrangian-based anal-  
866 ysis. *Meteor. Z.*, **24** (3), 225–242.
- 867 Zängl, G., D. Reinert, P. Rípodas, and M. Baldauf, 2015: The icon (icosahedral non-hydrostatic)  
868 modelling framework of dvd and mpi-m: Description of the non-hydrostatic dynamical core.  
869 *Quart. J. Roy. Meteor. Soc.*, **141** (687), 563–579.
- 870 Zhang, F., C. Docan, M. Parashar, S. Klasky, N. Podhorszki, and H. Abbasi, 2012: Enabling in-  
871 situ execution of coupled scientific workflow on multi-core platform. *Parallel & Distributed*  
872 *Processing Symposium (IPDPS), 2012 IEEE 26th International*, IEEE, 1352–1363.
- 873 Zuras, D., and Coauthors, 2008: Ieee standard for floating-point arithmetic. *IEEE Std 754-2008*,  
874 1–70.

## 875 **Sidebar: Domain-specific languages explained**

876 A domain-specific language (DSL) is a language specialized to a specific application domain,  
877 in our case the dynamical cores of weather and climate models. To illustrate the power of DSLs,  
878 two implementations of a simple fourth-order horizontal diffusion operator are given below (see  
879 Figure 9). The code on the left is an abridged Fortran implementation extracted from a climate  
880 model. The original optimized version entails significantly more code to specify parallelism, data  
881 placement, and data movement. The code on the right shows an implementation in the *gtclang*  
882 (<https://github.com/MeteoSwiss-APN/gtclang>) high-level DSL which is part of the Grid-  
883 Tools Framework. The code shown corresponds to the complete code implemented by the domain  
884 (climate) scientist. Details of how data is stored in memory and order of iteration over the com-  
885 putational grid are no longer visible. The responsibility to generate optimized, parallel code for a  
886 specific hardware architecture is delegated to the DSL compiler. As a result, the DSL implementa-  
887 tion is very concise and maintainable. DSLs vary in the level of abstraction. In the example shown,  
888 the responsibility to choose an appropriate numerical scheme for the Laplacian remains with the  
889 domain scientist. A DSL with a higher level of abstraction may hide the choice of numerics as  
890 well as computational grid from the user.

891 **LIST OF TABLES**

892 **Table 1.** Data volumes of the CMIP6-DECK simulations. (Third column) Estimate by  
893 the Centre for Environmental Data Analysis for a simulation employing a grid  
894 spacing of 0.5°, 40 model levels in the atmosphere and 60 levels in the ocean  
895 (Jukes et al. 2015; CEDA 2018). (Fourth column) The same output list pro-  
896 jected to an R2B11 mesh of the ICON model, employing 1.25 km grid spacing,  
897 180 levels in the atmosphere and 200 levels in the ocean ( $\times 6576$ ). (Fifth col-  
898 umn) Total data volume available for analysis for the 1.25 km simulation (foot-  
899 print of 2.9 TB in single-precision floating-point format), accounting for all 3D  
900 prognostic variables (8 in the atmosphere and 5 in the ocean) at each model  
901 time step (10 s). Adding all the available 2D fields (e.g., sea ice, soil, vege-  
902 tation) would amount to about an additional 3D variable. The CMIP6 DECK  
903 simulations (first two columns, from top to bottom) include a pre-industrial  
904 control simulation, an atmospheric model intercomparison simulation, a simu-  
905 lation forced by a 1%/yr CO<sub>2</sub> increase, and a simulation with abrupt quadru-  
906 pling of CO<sub>2</sub>. . . . . 44

Simulation	Length [yr]	CMIP6 @ 0.5° [TB]	CMIP6 @ 1.25 km [PB]	Data @ 1.25 km [ZB]
piControl	500	5	16.2	4.5
amip	36	1.7	1.3	0.4
1pctCO <sub>2</sub>	150	1.6	5.3	1.4
abrupt-4×CO <sub>2</sub>	150	8	22.2	1.4

907 TABLE 1. Data volumes of the CMIP6-DECK simulations. (Third column) Estimate by the Centre for Envi-  
908 ronmental Data Analysis for a simulation employing a grid spacing of 0.5°, 40 model levels in the atmosphere  
909 and 60 levels in the ocean (Juckes et al. 2015; CEDA 2018). (Fourth column) The same output list projected  
910 to an R2B11 mesh of the ICON model, employing 1.25 km grid spacing, 180 levels in the atmosphere and 200  
911 levels in the ocean ( $\times 6576$ ). (Fifth column) Total data volume available for analysis for the 1.25 km simulation  
912 (footprint of 2.9 TB in single-precision floating-point format), accounting for all 3D prognostic variables (8 in  
913 the atmosphere and 5 in the ocean) at each model time step (10 s). Adding all the available 2D fields (e.g., sea  
914 ice, soil, vegetation) would amount to about an additional 3D variable. The CMIP6 DECK simulations (first two  
915 columns, from top to bottom) include a pre-industrial control simulation, an atmospheric model intercomparison  
916 simulation, a simulation forced by a 1%/yr CO<sub>2</sub> increase, and a simulation with abrupt quadrupling of CO<sub>2</sub>.

917 **LIST OF FIGURES**

918 **Fig. 1.** Approaching the target of global km-scale climate simulations, represented by the sun symbol (left-hand panel), by refining either the resolution of GCMs, or by expanding the computational domain of high-resolution RCMs. The horizontal axes represents the domain size (fraction of Earth’s surface covered by the simulations) and the vertical axes the grid spacing (km). A selection of available simulations are indicated by the data points (right-hand panel), showing simulations longer than 10 years in full colours, and short prototype simulations in faint colours. The green contours in the right-hand panel show lines of same computational load, assuming that the time step is refined such as to keep the CFL-number constant. Red symbols relate to RCMs: 1 = Knote et al. 2010; 2 = Kendon et al. 2014; 3 = Ban et al. 2014; 4 = Leutwyler et al. 2017; 5 = Liu et al. 2017; Prein et al. 2017; 6 = Bretherton and Khairoutdinov 2015; 7 = Fuhrer et al. 2018. Blue symbols relate to GCMs: a = CMIP1 models (IPCC 1995, average horizontal resolutions of models); b = CMIP3 models (IPCC 2001); c = CMIP5 models (IPCC 2013); d = Sakamoto et al. 2012; e = CMIP6 HighRes MIP (Haarsma et al. 2016), f = Neumann et al. 2019, g = DYAMOND simulations (Sato et al. 2019), h = Miyamoto et al. 2013. . . . . 47

933 **Fig. 2.** Comparison of the energy consumption to transfer a single 64-bit floating point number from different levels of cache (L1, L2, L3) and system memory (DRAM), and the energy consumption to execute a 64-bit arithmetic operation (addition, multiplication and fused multiply add). Data is for Intel Xeon X5670 and AMD Opteron 2435 processors, adapted from Molka et al. (2010). . . . . 48

938 **Fig. 3.** Data exchange in atmospheric models. In order to ensure numerical stability, the exchange of data in an atmospheric model must exceed that of the physical propagation in the real atmosphere. (left) In the real atmosphere information travels approximately with the speed of sound. Within an hour, an air parcel over Zurich will thus exchange information within a radius of about 1200 km. The data exchange in numerical models strongly depends upon the numerical formulation. For instance, in a split explicit scheme (middle), data will be exchanged within a radius about twice that size, while in a spectral model (right), data will be exchanged globally at each time step. . . . . 49

946 **Fig. 4.** Performance penalty of a bit-reproducible COSMO version (providing reproducibility across an Intel Xeon E5-2690 CPU and a Nvidia Tesla K80 GPU). The dynamics section (green) hardly shows any penalty. The physics (blue) suffers from a large penalty (almost 2.5 time slower) due to the constraints imposed upon the compiler to avoid instruction re-arrangement when the CPU is targeted. Nevertheless, the entire time loop (red) containing both sections displays only a moderate performance penalty. . . . . 50

952 **Fig. 5.** Overview of the rerun (versus store) approach using SimFS. The scientist runs the initial simulation (top left) that produces the restart files and during which a first online analysis can be performed. The restart files are made available to SimFS, which can use them to restart the model. Later, analysis applications (bottom left) are transparently interfaced to SimFS via common I/O libraries (e.g., netCDF, HDF-5) or by using the SimFS API. SimFS checks if a simulation output file requested by an application is available on the configured storage mediums (e.g., fast flash memories, mechanic disks, magnetic tapes). If the file is not available, SimFS runs the model in order to re-create the file, otherwise it lets the requesting application open it. . . . . 51

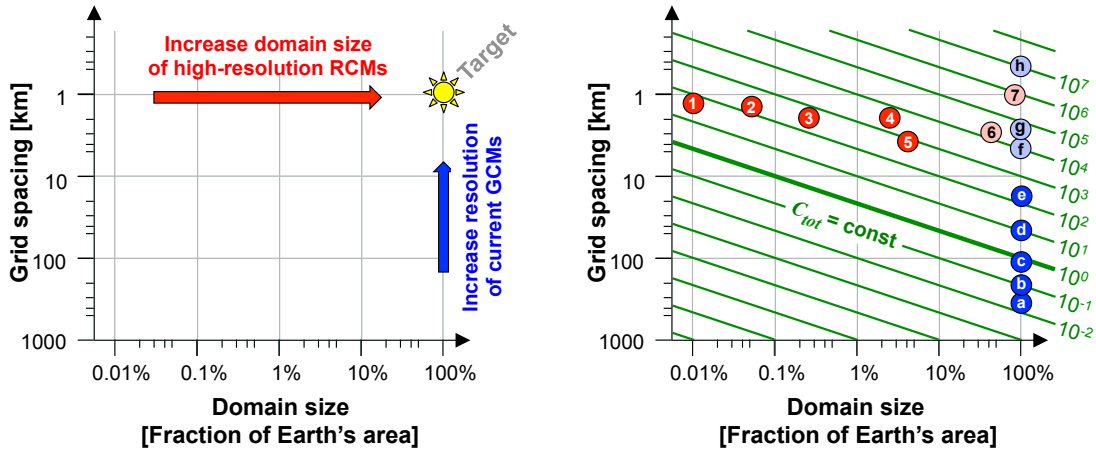
961 **Fig. 6.** Total cloud cover and precipitation over Europe obtained from convection-parameterizing (12 km horizontal grid spacing) and convection-resolving model simulations (2 km horizontal grid spacing) on July 2, 2009 at 15 UTC. The simulation snapshots demonstrate major

964 differences in the simulation of clouds and precipitation. Namely, the 12 km model shows  
965 widespread precipitation with low intensities and more clouds, while 2 km model simulates  
966 summer convection over Europe more realistically with more intense precipitation cells. The  
967 results are from a decade-long continental-scale simulation (Leutwyler et al. 2017). . . . 52

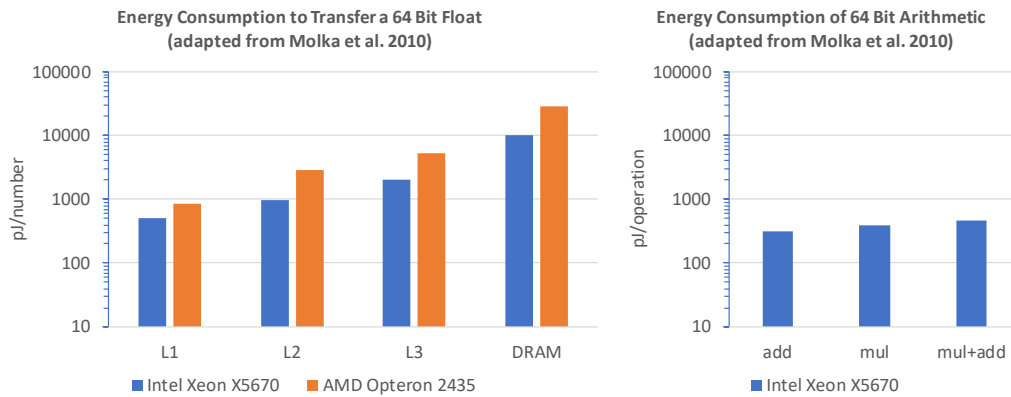
968 **Fig. 7.** Cloudiness in MODIS short-wave satellite observations (top right panel), compared against  
969 mid and low-level cloudiness in simulations at different horizontal resolutions (middle and  
970 bottom rows) on the 15th of December 2013. The simulation snapshots show the cloud  
971 cover fractions from convection-parameterizing simulations at 50 km and 12 km resolutions,  
972 and a convection-resolving simulation at 2 km resolution. The results are from month-long  
973 simulations driven by the ERA-Interim reanalysis initialized on November 25, 2013. Red  
974 and yellow circles pinpoint regions with large differences between simulations. The top left  
975 panel shows the geographical characteristics of the considered computational domains. . . . 53

976 **Fig. 8.** (a) Six-minute surface precipitation field ( $\text{mm h}^{-1}$ ) at 10 UTC 12 April 2000 in the entire  
977 domain, and (b) tracked precipitation cells at the same time over the Bay of Biscay. The  
978 symbols depict the current track event (star: genesis; cross: lysis; circle: continuation; right-  
979 pointing triangle: merging; left-pointing triangle: splitting; diamond: merging-splitting).  
980 The symbols and feature outlines are colored with the total cell lifetime (i.e., track duration).  
981 To indicate recent cell movement, the previous six positions of the track center are also  
982 shown. . . . 54

983 **Fig. 9.** Sidebar Figure: Comparison of a second-order Laplacian in Fortran (left) and *gtclang*  
984 (right). . . . 55

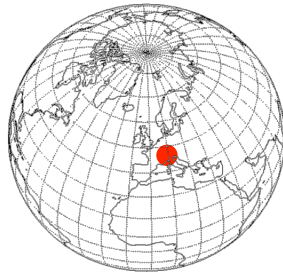


985 FIG. 1. Approaching the target of global km-scale climate simulations, represented by the sun symbol (left-  
 986 hand panel), by refining either the resolution of GCMs, or by expanding the computational domain of high-  
 987 resolution RCMs. The horizontal axes represents the domain size (fraction of Earth's surface covered by the  
 988 simulations) and the vertical axes the grid spacing (km). A selection of available simulations are indicated by  
 989 the data points (right-hand panel), showing simulations longer than 10 years in full colours, and short prototype  
 990 simulations in faint colours. The green contours in the right-hand panel show lines of same computational load,  
 991 assuming that the time step is refined such as to keep the CFL-number constant. Red symbols relate to RCMs: 1  
 992 = Knote et al. 2010; 2 = Kendon et al. 2014; 3 = Ban et al. 2014; 4 = Leutwyler et al. 2017; 5 = Liu et al. 2017;  
 993 Prein et al. 2017; 6 = Bretherton and Khairoutdinov 2015; 7 = Fuhrer et al. 2018. Blue symbols relate to GCMs:  
 994 a = CMIP1 models (IPCC 1995, average horizontal resolutions of models); b = CMIP3 models (IPCC 2001); c  
 995 = CMIP5 models (IPCC 2013); d = Sakamoto et al. 2012; e = CMIP6 HighRes MIP (Haarsma et al. 2016), f =  
 996 Neumann et al. 2019, g = DYAMOND simulations (Satoh et al. 2019), h = Miyamoto et al. 2013.

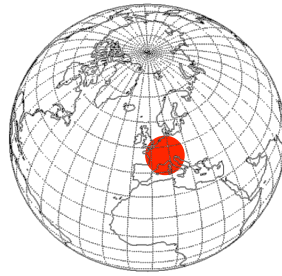


997 FIG. 2. Comparison of the energy consumption to transfer a single 64-bit floating point number from different  
 998 levels of cache (L1, L2, L3) and system memory (DRAM), and the energy consumption to execute a 64-bit  
 999 arithmetic operation (addition, multiplication and fused multiply add). Data is for Intel Xeon X5670 and AMD  
 1000 Opteron 2435 processors, adapted from Molka et al. (2010).

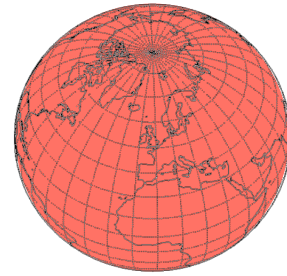




**Physical propagation  
in the real atmosphere**  
(ca 1200 km / hour)  
Speed of sound

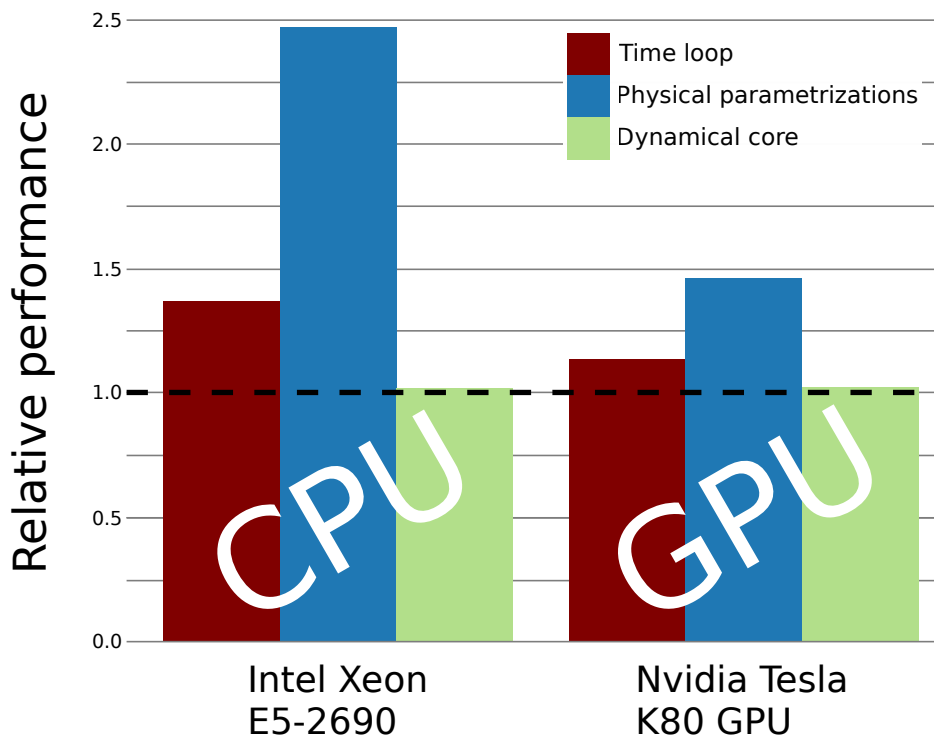


**Propagation of data  
in a split-explicit model**  
(ca 2000 km / hour)

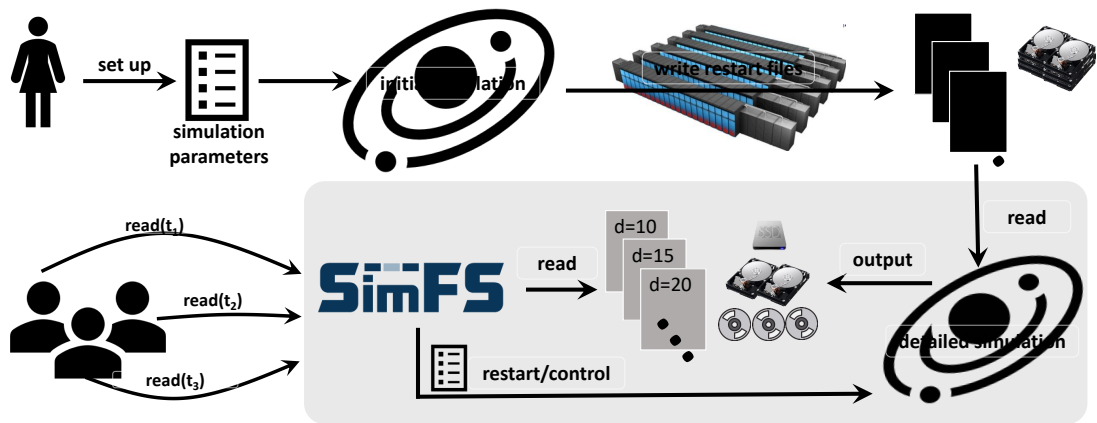


**Propagation of data  
in spectral models**  
(global communication  
at each time step)

1001 FIG. 3. Data exchange in atmospheric models. In order to ensure numerical stability, the exchange of data  
1002 in an atmospheric model must exceed that of the physical propagation in the real atmosphere. (left) In the  
1003 real atmosphere information travels approximately with the speed of sound. Within an hour, an air parcel over  
1004 Zurich will thus exchange information within a radius of about 1200 km. The data exchange in numerical models  
1005 strongly depends upon the numerical formulation. For instance, in a split explicit scheme (middle), data will  
1006 be exchanged within a radius about twice that size, while in a spectral model (right), data will be exchanged  
1007 globally at each time step.

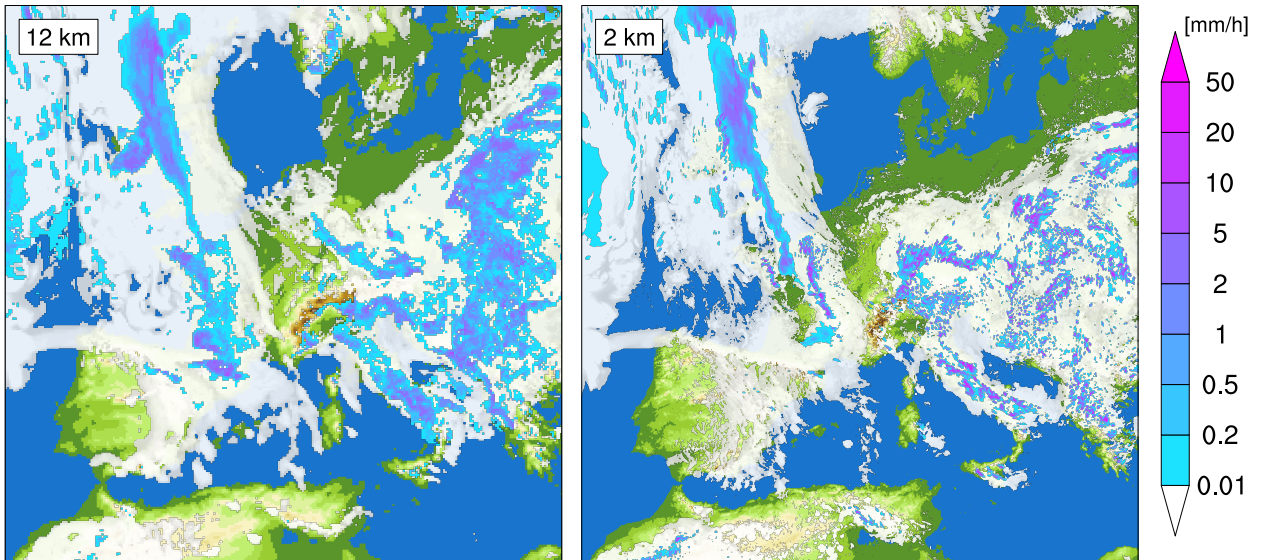


1008 FIG. 4. Performance penalty of a bit-reproducible COSMO version (providing reproducibility across an Intel  
 1009 Xeon E5-2690 CPU and a Nvidia Tesla K80 GPU). The dynamics section (green) hardly shows any penalty.  
 1010 The physics (blue) suffers from a large penalty (almost 2.5 time slower) due to the constraints imposed upon the  
 1011 compiler to avoid instruction rearrangement when the CPU is targeted. Nevertheless, the entire time loop (red)  
 1012 containing both sections displays only a moderate performance penalty.

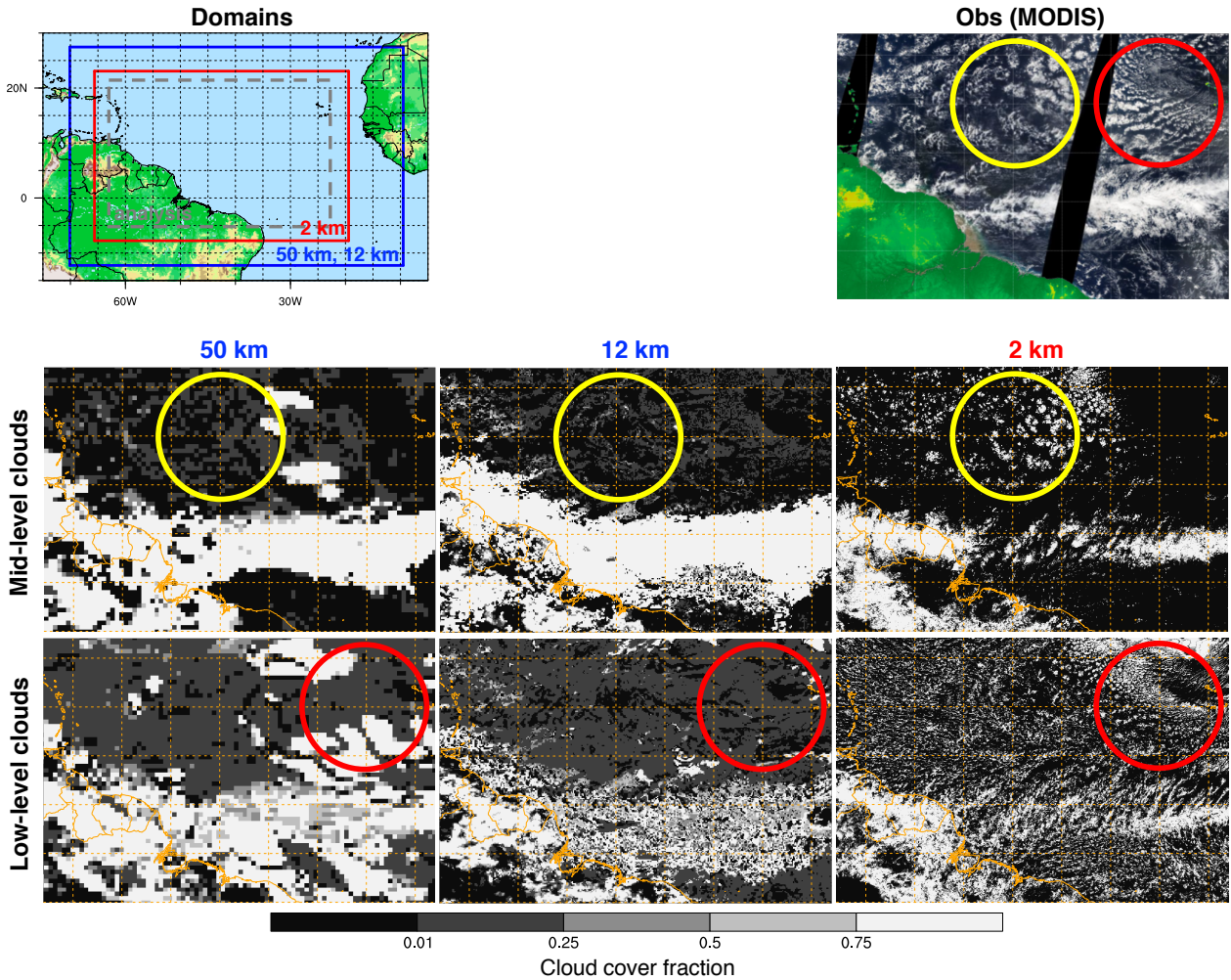


1013 FIG. 5. Overview of the rerun (versus store) approach using SimFS. The scientist runs the initial simulation  
 1014 (top left) that produces the restart files and during which a first online analysis can be performed. The restart files  
 1015 are made available to SimFS, which can use them to restart the model. Later, analysis applications (bottom left)  
 1016 are transparently interfaced to SimFS via common I/O libraries (e.g., netCDF, HDF-5) or by using the SimFS  
 1017 API. SimFS checks if a simulation output file requested by an application is available on the configured storage  
 1018 mediums (e.g., fast flash memories, mechanic disks, magnetic tapes). If the file is not available, SimFS runs the  
 1019 model in order to re-create the file, otherwise it lets the requesting application open it.

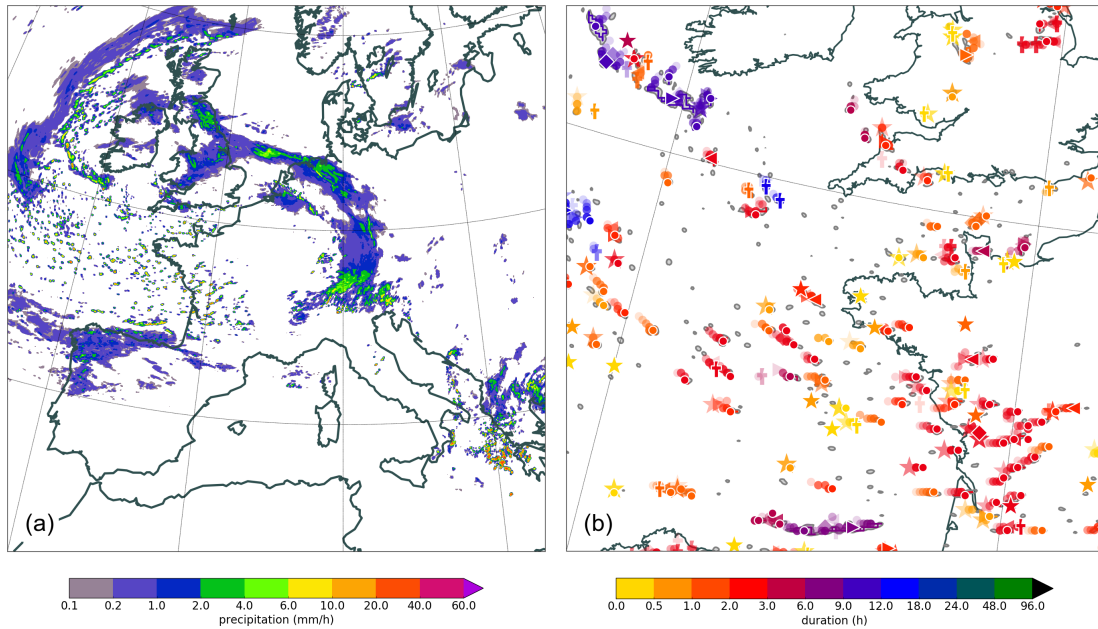
## Clouds and Precipitation on July 2, 2009 at 15 UTC



1020 FIG. 6. Total cloud cover and precipitation over Europe obtained from convection-parameterizing (12 km  
1021 horizontal grid spacing) and convection-resolving model simulations (2 km horizontal grid spacing) on July  
1022 2, 2009 at 15 UTC. The simulation snapshots demonstrate major differences in the simulation of clouds and  
1023 precipitation. Namely, the 12 km model shows widespread precipitation with low intensities and more clouds,  
1024 while 2 km model simulates summer convection over Europe more realistically with more intense precipitation  
1025 cells. The results are from a decade-long continental-scale simulation (Leutwyler et al. 2017).



1026 FIG. 7. Cloudiness in MODIS short-wave satellite observations (top right panel), compared against mid and  
 1027 low-level cloudiness in simulations at different horizontal resolutions (middle and bottom rows) on the 15th  
 1028 of December 2013. The simulation snapshots show the cloud cover fractions from convection-parameterizing  
 1029 simulations at 50 km and 12 km resolutions, and a convection-resolving simulation at 2 km resolution. The  
 1030 results are from month-long simulations driven by the ERA-Interim reanalysis initialized on November 25,  
 1031 2013. Red and yellow circles pinpoint regions with large differences between simulations. The top left panel  
 1032 shows the geographical characteristics of the considered computational domains.



1033 FIG. 8. (a) Six-minute surface precipitation field ( $\text{mm h}^{-1}$ ) at 10 UTC 12 April 2000 in the entire domain,  
 1034 and (b) tracked precipitation cells at the same time over the Bay of Biscay. The symbols depict the current track  
 1035 event (star: genesis; cross: lysis; circle: continuation; right-pointing triangle: merging; left-pointing triangle:  
 1036 splitting; diamond: merging-splitting). The symbols and feature outlines are colored with the total cell lifetime  
 1037 (i.e., track duration). To indicate recent cell movement, the previous six positions of the track center are also  
 1038 shown.

```

subroutine horizontal_diffusion(in, out, ie, je, ke)
  implicit none

  real, intent(in) :: in(-1:ie+2, -1:je+2, ke)
  real, intent(out) :: out(-1:ie+2, -1:je+2, ke)

  real :: lap(0:ie+1, 0:je+1)
  integer :: i, j, k

  do k = 1, ke

    do j = 0, je+1
      do i = 0, ie+1
        lap(i,j,k) = 4.0 * in(i,j,k) - in(i+1,j,k) - in(i-1,j,k) &
          - in(i,j+1,k) - in(i,j-1,k)
      end do
    end do

    do j = 1, je
      do i = 1, ie
        out(i,j,k) = out(i,j,k) - 0.1 * (
          4.0 * in(i,j,k) - in(i+1,j,k) - in(i-1,j,k) &
          - in(i,j+1,k) - in(i,j-1,k) )
      end do
    end do

  end do
end subroutine horizontal_diffusion

```

```

stencil_function laplacian {
  storage phi;
  Do {
    return 4.0 * phi - phi[i+1] - phi[i-1]
      - phi[j+1] - phi[j-1];
  }
}

stencil horizontal_diffusion {
  storage out, in;
  temporary_storage lap;
  Do {
    vertical_region(k_start, k_end) {
      lap = laplacian(in);
      out = out - 0.1 * laplacian(lap);
    }
  }
}

```

FIG. 9. Sidebar Figure: Comparison of a second-order Laplacian in Fortran (left) and *gtclang* (right).

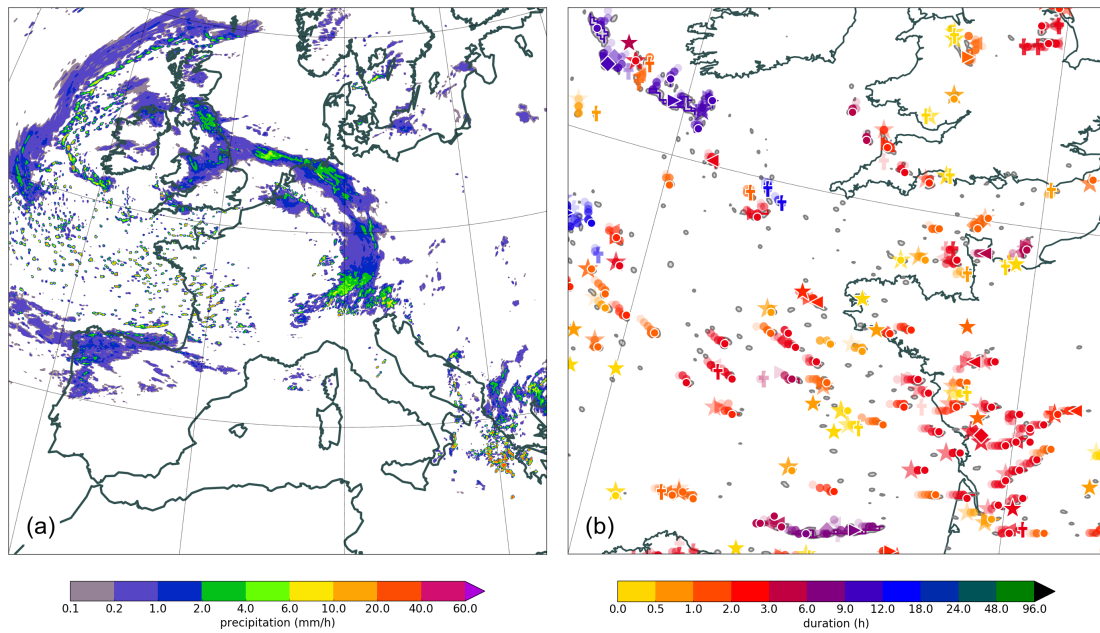
Supplementary Information for "Kilometer-scale climate models:  
Prospects and challenges"

by Christoph Schär et al.



Supplementary Table 1: List of compiler flags used to control mathematical expressions rearrangement for a given target architecture/compiler. The flags with \* generate compilation errors depending on the compiler version. In that case the default was used (shown in parenthesis if available).

Compiler	CPU	GPU
Cray	-O0, -hfp0, -hflex_mp=intolerant, -hnoacc, -hnoaggress, -hnoautothread, -hfusion0, -hnopattern	-O1* (-O2), -hfp0, -hacc, -hnoaggress, -hnoautothread, -hfusion0, -hnopattern, -hflex_mp=strict* (=default)
GNU	-fno-fast-math, -O0, -fno-builtin, -fno-rounding-math, -fno-reciprocal-math, -ffp-contract=off, -march=native	N/A
Nvidia	N/A	--fmad=false



Supplementary Figure 1: 12-h backward trajectories arriving in the upper Rhine valley at Vaduz between the surface and 1000 m above ground at 200 m height intervals. The arrival time corresponds to 21 UTC 14 April 2000 in the upper row, and one hour later in the lower row. The four panels in each row show the results when using different input intervals of the driving 3D winds: 1, 5, 20, 60 min from left to right. Whereas the northerly flow at 21 UTC is similarly captured when using different wind field intervals, the situation is more complex one hour later after the onset of the southerly Foehn. The most accurate computation, using wind fields every 1 or 5 min, reveals that the flow originates from the region of Davos, while with winds every 20 or 60 min the air parcels enter the Rhine valley much earlier and further south.